Review

Hybrid Nanostructured Magnetite Nanoparticles: From Bio-Detection and Theragnostics to Regenerative Medicine

Yolanda Piñeiro *, Manuel González Gómez, Lisandra de Castro Alves, Angela Arnosa Prieto, Pelayo García Acevedo, Román Seco Gudiña, Julieta Puig, Carmen Teijeiro, Susana Yáñez Vilar * and **José Rivas**

Applied Physics Department, Nanomag Laboratory, Universidade de Santiago de Compostela, 15782 Santiago de Compostela, Spain; manuelantonio.gonzalez@usc.es (M.G.G.); lisandracristina.decastro@usc.es (L.d.C.A.); angela.arnosa@usc.es (A.A.P.); pelayo.garcia.acevedo@usc.es (P.G.A.); romanseco@hotmail.es (R.S.G.); julieta.puig@usc.es (J.P.); carmen.teijeiro@usc.es (C.T.); jose.rivas@usc.es (J.R.)
* Correspondence: y.pineiro.redondo@usc.es (Y.P.); susana.yanez@usc.es (S.Y.V.); Tel.: +34-881813062 (Y.P.); +34-881813062 (S.Y.V.)

check for updates

Abstract: Nanotechnology offers the possibility of operating on the same scale length at which biological processes occur, allowing to interfere, manipulate or study cellular events in disease or healthy conditions. The development of hybrid nanostructured materials with a high degree of chemical control and complex engineered surface including biological targeting moieties, allows to specifically bind to a single type of molecule for specific detection, signaling or inactivation processes. Magnetite nanostructures with designed composition and properties are the ones that gather most of the designs as theragnostic agents for their versatility, biocompatibility, facile production and good magnetic performance for remote in vitro and in vivo for biomedical applications. Their superparamagnetic behavior below a critical size of 30 nm has allowed the development of magnetic resonance imaging contrast agents or magnetic hyperthermia nanoprobes approved for clinical uses, establishing an inflection point in the field of magnetite based theragnostic agents.

Keywords: magnetite; superparamagnetism; biodetection; magnetofection; imaging; therapy; tissue engineering

---

1. Introduction

Magnetism has been technologically exploited for centuries, well before quantum mechanics helped to unveil the fundamental mechanisms governing the behavior of magnetic materials.

Electrical steels, permanents magnets, nickel-iron alloys or soft ferrites mechanized in different configurations just from bulk, ribbon or disks are the enabling materials behind disparate developments like compasses for marine navigation, bulk magnetic separation devices in mining industry, inductive heating in massive foundry industry, sophisticated devices for electric power generation and distribution or communications and information storage in hard disks [1].

The large variety of applications exploiting different aspects of magnetism has permeated our technically developed society in the last decades and follows still an intense evolution by the hand of applications based on magnetic materials tailored at the nanometric scale. In fact, the optimization and maturity of chemical synthetic procedures during the last decades has allowed the development of materials with designed properties which are only observable at the nanoscale such as, surface plasmonic resonance, enhanced and specific catalytic activity, size-dependent fluorescence,

superparamagnetism [2], quantum tunneling magnetization [3] or enhanced coercivity [4] that, all combined, open the door to highly interesting biomedical and technological applications.

In addition to their designed properties, magnetic nanoparticles (MNPs) are an intense topic of research in diagnostic, theragnostic and regenerative medicine applications, due to their small size, which is comparable to relevant cell length scales and allows to interact and interfere with biological processes, minimizing adverse effects and opening the way to new diagnostic and therapeutic paradigms [5].

Specifically, superparamagnetic iron oxides nanoparticles (SPIONs) are witnessing a predominant role in nanomedicine developments relaying on their biocompatibility, unbeatable low cost production, physicochemical performance and versatile chemistry that make them almost universally present as a main components in contrast agents for magnetic resonance imaging (MRI), magnetic hyperthermia sources or drug delivery nanoplatforms [6].

It is striking, however, that Nature had incorporated crystalline magnetite nanoparticles (NPs) as a strategy for magnetic guiding in small animals, thousands of years before the recent developments of nanotechnology. Magnetotactic bacteria, bees or pigeons are equipped with magnetic dipolar arrays of small Fe_3O_4 NPs, biologically synthesized in specific vesicles, that serve as natural compasses to orientate in the magnetic field of the Earth. Moreover, magnetite NPs can be found also in humans, when a pathologically altered iron metabolism triggers their synthesis inside ferritin (Fn), a spherical hollow protein in charge of delivering Fe^{3+} to feed our cell biomachinery [7].

Besides its good magnetic performance (Curie temperature well above any biomedical application, large values of initial susceptibility and saturation magnetization) and biocompatibility, the availability of facile wet chemistry techniques to produce superparamagnetic (SPM) cores with well controlled size, shape and composition has promoted magnetite to the most relevant position in the field of nanomedicine for biodetection, imaging and therapy.

In fact, it competes with the most well accepted soft organic compounds, like liposomes or nano-emulsions, fully biocompatible, biodegradable with enhanced ability for encapsulating a variety of hydrophilic or lipophilic drugs [8] that have found approval for clinical uses in a variety of applications as vaccines, antifunghical, anesthetics or antibiotics [9]. Although with a slower pace, a few set of superparamagnetic magnetite NPs have been clinically tested and approved for commercialization as enhanced contrast agents for magnetic resonance imaging (Feridex; Resovist, Ferumoxtran) [10] or magnetic hyperthermia therapies for brain tumor treatment (NanoTherm) [11], establishing an inflection point in the use of inorganic materials as theragnostic agents.

By simple and scalable methods like co-precipitation, hydrothermal or solvothermal decomposition procedures, easy production of spheres, cubes, hexagons, octahedra, hollow spheres, rods, plates or wires can be obtained with controlled size. Combined with surface functionalization procedures, these magnetite NPs can be engineered to produce multifunctional hybrid nanostructures with a designed composition of inorganic/organic/biological shells containing carbon, metal (Au, Ag, Cu, etc.), metal oxides (Ti, Si, Zr, etc.), hydroxides (Al, etc.), organic compounds (polymers like polyacrylic acid (PAA), polyethylene glycol (PEG), etc.), short organic molecules (OAc, dopamine, etc.) and biological moieties (antibodies, aptamers, plasmids, etc.) [12].

This core-shell strategy has given rise to different configurations like single- and multi-core@shell nanoparticles, where magnetite is located in the core ($Fe_3O_4@SiO_2$; $Fe_3O_4@C$), in the shell (gelatin-NPs@Fe_3O_4-NPs) or embedded in a polymer matrix (polyester, gelatin magnetic beads). In all cases, the nanostructure inherits a combination of abilities that ensures their multimodal capacities for simultaneous magnetic separation/detection/targeting procedures like contrast agents in magnetic resonance imaging/positron emission tomography (MRI/PET), magnetic hyperthermia (MH)/drug delivery therapeutic agents, among others [12].

Moreover, magnetite based nanostructures can be also included as the magnetic phase in a nanocomposite material like mesoporous silica, biopolymer sponges (chitosan, k-carrageenan, alginate, etc.), porous stiff materials (hydroxyapatite, polycaprolactone, etc.) or hydrogels, allowing to produce

magnetic scaffolds for tissue engineering combining all the theragnostic abilities, inherited from magnetite, together with magnetic cell growth stimulation or magnetic external fixation [13].

The list of nanostructured materials containing magnetite NPs is huge, and the applications in nanomedicine cover almost any aspect from detection, diagnosis and therapy to regenerative medicine.

In this work, we present the structure, properties, synthetic procedures and applications emerging from the magnetically intrinsic properties of magnetite nanostructures with tailored configuration, size and shape.

2. Magnetite: Structure and Properties from Bulk to Nanoscale

Magnetite, Fe_3O_4, is an iron oxide compound where iron ions (with valence 3+ and 2+) adjust to the $AB_2O_4 = Fe^{3+} (Fe^{2+}Fe^{3+})O_4$ formulation, arranged in an inverse-spinel crystal structure [14], composed by tetrahedral, A, and octahedral, B, sublattices. The magnetic and electric properties of magnetite arise from the interactions between the Fe^{3+} (d^5) and Fe^{2+} (d^6) ions placed on octahedral positions and Fe^{3+} (d^5) ions on tetrahedral positions. The spinel is a stable crystal structure that accepts the substitution of the A and B lattice locations by a variety of nearly 30 different metal ions with valences ranging from +1 to +6. An example of this stability is the fact that both, natural magnetite is commonly found containing impurity ions (Ti, Al, Mg, and Mn), and substituted ferrites containing transition metals (Co, Mn, Zn) can be easily obtained by wet chemistry procedures [15]. The unit cell in bulk Fe_3O_4 consists in a face centered cubic, fcc, (Fd^3m space group) arrangement of O^{2-} ions, in which Fe^{3+} (d^5) cations occupy 1/2 of the tetrahedral interstices, and a 50:50 mixture of Fe^{3+} (d^5) and Fe^{2+} (d^6) cations occupy 1/8 of the octahedral interstices, with a characteristic unit cell parameter ≈ 8.4 Å (see Figure 1).
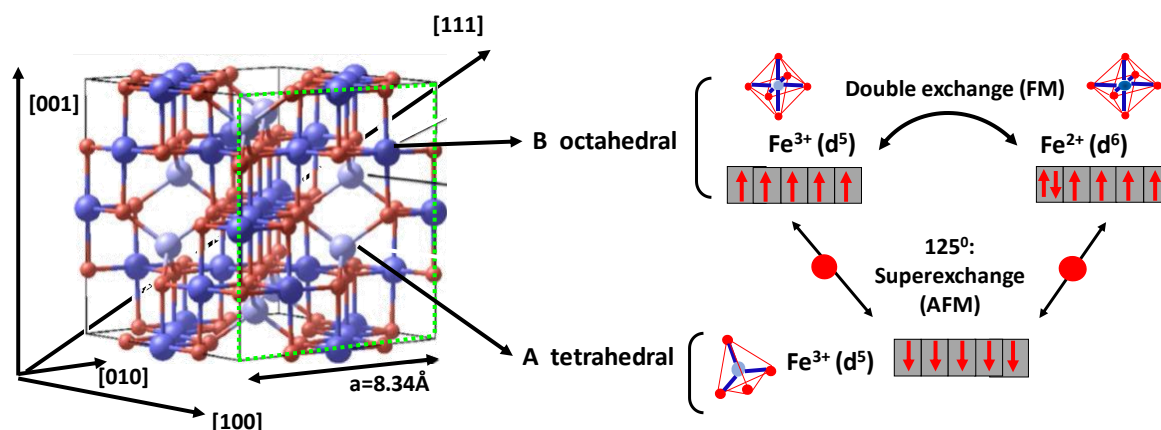

Figure 1. On the left, the inverse spinel structure (crystal structure adapted from [16] (Science Direct, 2016), of Fe_3O_4 is based on a face centered cubic (fcc) arrangement of O^{2-} ions in which Fe^{3+} (d^5) cations occupy 1/2 of the tetrahedral interstices, and a 50:50 mixture of Fe^{3+} (d^5) and Fe^{2+} (d^6) cations occupy 1/8 of the octahedral interstices. On the right, the set of exchange interactions between Fe^{3+} (d^5), Fe^{2+} (d^6) and O^{2-} ions, giving rise to ferrimagnetic ordering.

At temperatures above 118 °K, Fe^{2+} and Fe^{3+} ions are randomly distributed over the octahedral sites allowing electron hopping between them and giving rise to the low electrical resistivity, around 7 mili-Ohm/cm at T_{room}, of magnetite [15]. Below 118 °K, the Fe^{3+} and Fe^{2+} ions become ordered following a cubic to orthorhombic crystallographic transition, as proposed by Verwey [17], where c axis of the new orthorhombic phase is parallel to and slightly smaller than the cube edge of the fcc phase and accompanied by electronic charge ordering of the Fe^{3+} and Fe^{2+} ions on the B sites, which produces a large increase in resistivity [18].

The magnetic ordering in magnetite is dominated by the specific distribution of Fe^{3+} and Fe^{2+} ions on both A and B sites, and the exchange interactions originated when the 3d electron orbital

of the Fe ions overlap with the 2p electron orbital of O^{2-} ions, since direct exchange between Fe-Fe interactions are negligible due to the large distance between Fe ions [19]. Fe-O-Fe super-exchange interaction depends on the distance and angle of bonds between the Fe^{3+} and Fe^{2+} and O^{2-} ions and is responsible for antiparallel alignment of the net magnetic moment of A and B sublattices, which gives rise to the ferrimagnetic order in magnetite [15]. As proposed by Neel, Fe^{3+} ions on the oppositely aligned tetrahedral and octahedral cancel each other, and only the remaining magnetic moment of Fe^{2+} ions contributes to the total magnetic moment of magnetite (see Figure 1).

Moreover, the spin magnetic moments, which are tied to their electron orbit by the spin–orbit interaction, orientate themselves into specific directions in the lattice that minimize the crystalline field and give rise to the magnetic anisotropy axes. In magnetite, easy (low-energy), hard (high-energy) and intermediate (medium-energy) magnetocrystalline anisotropy directions are defined by the cubic lattice axes [111], [100] and [110], respectively (see Figure 1) [15]. At low temperatures, 118 °K, the crystallographic transition from cubic to orthorhombic provokes the appearance of a magnetic isotropic point where the anisotropy constant (K1) sign changes from − to +, (K1 = 0) and is known as the Verwey transition.

Compared to other permanent magnetic materials (see Table 1), [20] magnetite shows a low effective magnetocrystalline anisotropy constant, high saturation magnetization per unit mass ($M_S \sim 92$ emu/g), low coercivity ($H_C = 10$–40 mT) and high Curie temperature ($T_C = 850°$) compared to relevant temperatures for biomedical applications, and a molecular magnetic moment of 4.1 μ_{Bohr} (accounting for the larger Fe^{2+} contribution) [15].

Table 1. Bulk magnetocrystalline anisotropy constant, K_{an}, Curie temperature, Tc, for representative magnetic materials. Data compiled from data included in [20].

Material	Fe	Co	Ni	PtFe	Fe_3O_4	γ-Fe_2O_3
K_{an} (kJ/m^3)	48	530	4.8	6600	11	4.6
T_C (K)	1043	1388	631	750	858	863

However, besides the specific crystalline structure of different magnetic materials, there is one common fact that affects their main magnetic behavior: size.

In order to accommodate all the magnetic interaction terms (exchange, Zeeman, demagnetizing field and anisotropy) bulk materials attain stability by adopting a magnetic configuration of multidomains separated by domain walls, that minimizes the total magnetic free energy [21]. When preparing small particles with sizes down to the nanometer scale, the balance of magnetic interaction terms changes: the energy cost of introducing domain walls is higher than the reduction of demagnetizing field, the anisotropy energy decreases proportionally to the reduction in volume of the particle, and single domain becomes the most stable magnetic configuration [22]. This multidomain to single domain transition happens for particles with a critical radius in the nanometer scale, ($R_C = 10$–100 nm), and depends on the material properties as $R_C = 36 \sqrt{AK}/\mu_0 M_s^2$ (A, exchange constant, K, anisotropy constant and Ms, saturation magnetization) [23].

Fe_3O_4 NPs undergo a transition from multi- to single-domain magnetic structure 80–90 nm, and by further size reduction, which in magnetite happens between 25 to 30 nm, another transition arises when the total anisotropy energy of the crystallite becomes smaller than thermal energy. This fact originates that, in absence of externally applied magnetic fields, the magnetization (M) spontaneously fluctuates at room temperature by thermal stimulation and, in average, M equals zero. This is the so called superparamagnetic regime, characterized by negligible remanence or coercive forces (Figure 2a) and reversible magnetization with a rapid "on–off" magnetic switching, modulated by the initial magnetic susceptibility (χ_{in}) (in magnetite NPs can range from: $\chi_{in} = 0.5$–1) [24].

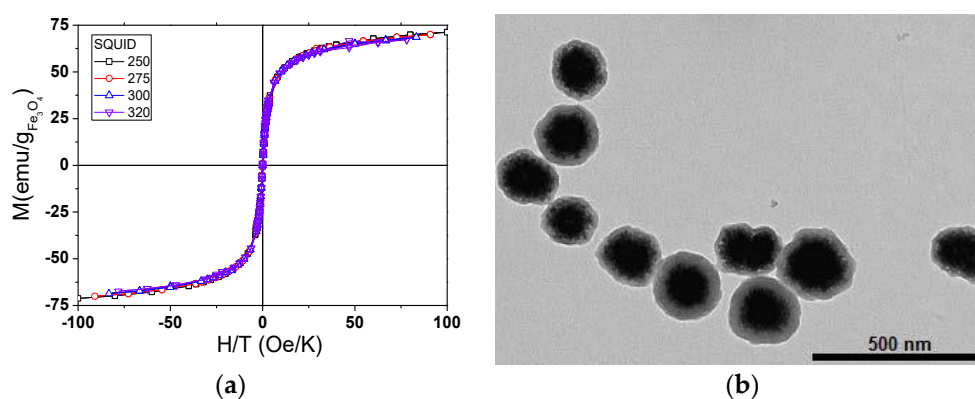(a)   (b)

Figure 2. (**a**) Overlapping into a single curve of magnetization data versus H/T, that correspond to measurements performed corresponding from 250 to 320 K, on a dried sample of SPM multi-core Fe$_3$O$_4$@C, showing negligible remanence and coercive forces and (**b**) Transmission electron microscopy (TEM) micrograph of multi-core Fe$_3$O$_4$ @C, with averaged size 187 nm. (Figures reprinted with permission from [25], IEEE, 2016).

Chemical procedures like coprecipitation, thermal decomposition or hydrothermal preparations, are the most used wet chemistry techniques to provide high quality and monodisperse SPIONs with diameters ranging from 10 to 30 nm that have become a standard material as magnetic hyperthermia actuators with high specific absorption rates (SAR) in clinical applications (MAGFORCE-NanoTherm) [11] or as T2 MRI commercial contrast agents (Feridex; Resovist, Ferumoxtran [10]).

In addition, SPM behavior can be preserved in multi-core configurations (see Figure 2b) even though several magnetic cores stand in close contact embedded inside a coating shell (see Figure 2) [25]. These NPs are particularly interesting for those applications that require a high concentration of magnetic material in a small region to ensure an intense magnetic response (i.e., cell isolation purposes). The key procedure consists in coating the single-core magnetite surfaces to avoid exchange interaction between them that may cause exchange bias, commonly resulting in reduced saturation magnetization, low initial magnetic susceptibility or the loss of SPM behavior.

However, associated with the size reduction, the increase of surface-to-volume ratio (typically, for 5 nm NPs, the surface spins represent 30% of total amount of spins [26]), entails the dominant contribution of surface properties, incorporating a crucial problem for magnetic applications: the reduction of saturation magnetization [27]. For very small magnetic NPs, a surface dead magnetic layer appears related to specific features like:

1. The large contribution of surface ions, located on edges or corners, with coordination numbers lower than inner core ions, (see Figure 3) gives rise to an abrupt breakdown of the lattice and magnetic symmetry, which induces changes in magnetic anisotropy at the surface.
2. The chemical environment of the coating shell influences the magnetic properties of the surface ions.
3. The interaction of the surface spins with the inner ones by an exchange bias may lead to some degree of frustration that lowers the total magnetization of the nanoparticle [28].
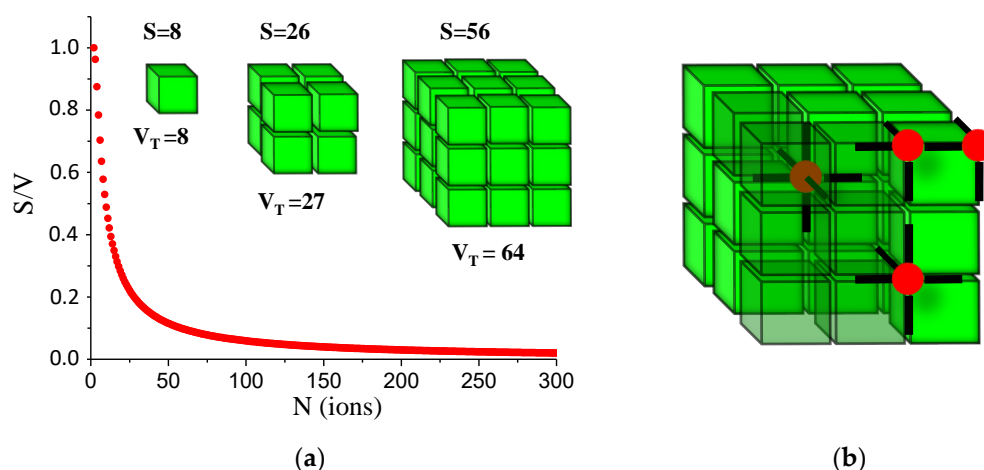
Figure 3. (**a**) Ratio of surface to volume ions in a cubic lattice, for very small nanoparticles (NPs) surface ions can amount up to large percentages of the totality and (**b**) corner, edge, surface and inner ions with different coordination numbers.

Although the preservation of optimum magnetic properties in small magnetic particles through the increase of crystalline quality and minimization of surface distortion has witnessed a large effort in chemical approaches in the last years [29], the production of pure colloidal SPIONs remains a challenge. Magnetite cores with a thin overoxidized (Fe^{3+}) surface shell, compositionally close to a maghemite polymorph (γ-Fe_2O_3), are normally obtained and only synthetic procedures driven at high temperatures can improve the purity and crystallinity of colloidal SPIONs with enhanced saturation magnetization (M_S = 70–85 emu/g) [30].

3. Synthetic Procedures of Multifunctional SPM Magnetite Nanostructures

For in vitro or in vivo applications, not only the magnetic core, but also the capping ligands on the surface, are the crucial aspects to ensure an adequate performance of the magnetic nanostructures when they interact with biological media, like fluids or tissues, where they can be critically arrested.

However, besides the efforts devoted to produce multifunctional magnetite nanostructures with high quality, the requirements to ensure a good in vitro and in vivo performance include a biocompatible coating and an adequate solvent dispersant, and for in vitro and in vivo applications is crucial to maintain colloidal stability of the preparations. Therefore, the chemical engineering to prepare SPIONs with several added functionalities requires a hierarchical procedure involving the production of good quality magnetite cores and several functionalization steps to add plasmonic NPs, fluorescent moieties, biological agent or biocompatible coating shells.

3.1. Synthesis of the Magnetic Core. Synthetic Procedures Modulating Size and Shape

With the aim of producing magnetite NPs with exceptional magnetic specifications, high crystalline quality, well-controlled size and shape, and easy procedures, different wet chemistry approaches have been studied based on co-precipitation, thermal decomposition, solvothermal or hydrothermal techniques (summarized in Figure 4). In combination or alone, they can be conveniently modified to produce magnetite NPs with different morphologies (spheres, cubes, hexagons, octahedra, hollow spheres, etc.), high crystalline quality, different architectures of single- or multiple-core configurations [31] or to provide large gram-scale production of NPs [32]. These techniques have allowed the development of SPIONs spanning from 10 nm to several hundreds of nanometers.
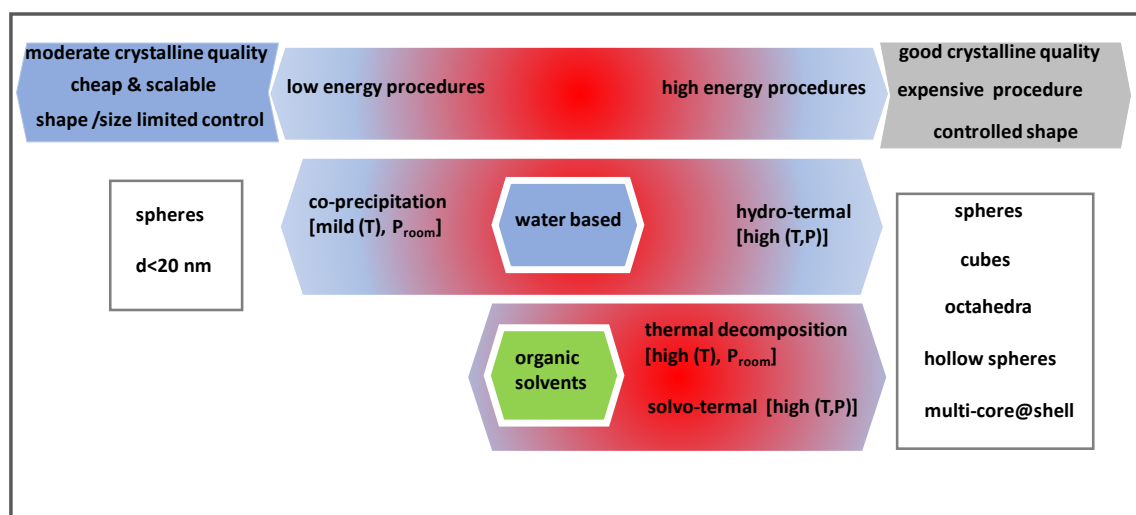
Figure 4. Summary of synthetic routes commonly used to produce superparamagnetic iron oxides nanoparticles (SPIONs).

3.1.1. Precipitation Methods

Precipitation methods of iron salts in a highly basic solution are easy, fast, scalable and can be done at low to moderate temperatures and inert atmosphere. Co-precipitation of two iron Fe^{2+}/Fe^{3+} salt precursors can be easily controlled by experimentally adjusting the Fe^{2+}/Fe^{3+} ions ratio, pH and temperature, providing spherical NPs with a good control of the structural (size, morphology) (see Figure 5a) and magnetic properties but a with wide size distribution. Although its easiness has made this basic method very popular, the ensembles produced in this way inherit a distribution of blocking temperatures, undesired in certain in vivo applications [33] or a distribution of magnetic moments that need to be avoided for magnetic detection kits.
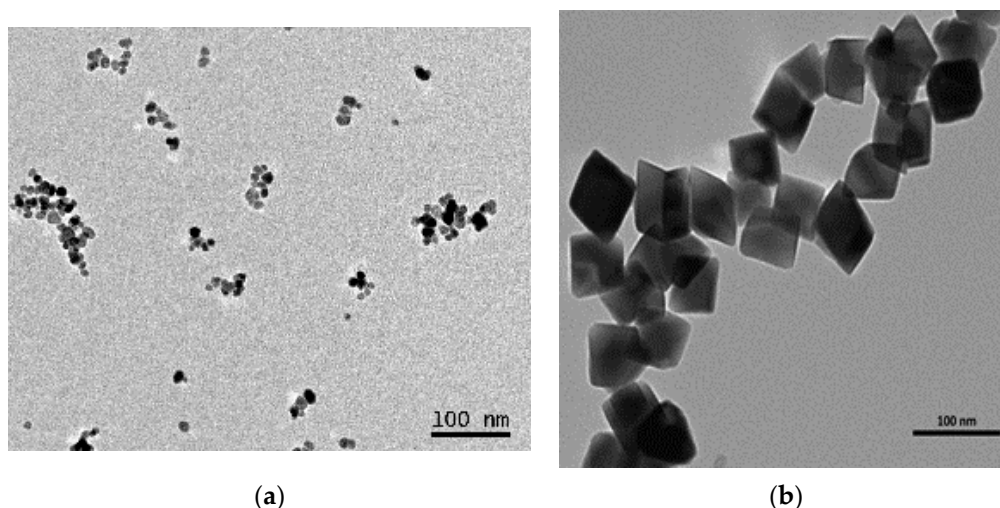

(**a**)   (**b**)

Figure 5. TEM image of (**a**) spherical magnetite NPs coated with citrated and obtained by a coprecipitation method and (**b**) bare cubic magnetite NPs obtained by a precipitation method.

Related to these needs, optimized co-precipitation procedures have been implemented attending to fundamental chemistry facts: reaction kinetics, atmosphere and temperature control. Following the general theory of nucleation and growth, under the so-called burst nucleation approach, a monodisperse solution of "nuclei" can be obtained by using supersaturated solutions of the precursors to nucleate in

a fast and homogenous way. Furtherly, imposing a slow pace at the growth stage, a monodisperse ensemble of NPs can be achieved [34].

In addition, since magnetite easily oxides into hematite (Fe_2O_3), a non-magnetic iron oxide phase, applying inert conditions to the reaction, with a controlled oxygen atmosphere, avoids the formation of Fe_2O_3 and γ-Fe_2O_3, the other ferrimagnetic oxide.

Moreover, crystalline quality can be optimized by supplying energy to facilitate the annealing of the magnetite lattice. A modified technique [35], based on the precipitation of a single iron salt in a basic solution and a free oxygen atmosphere, allows to obtain $Fe(OH)_2$, which after heating at 363 K in a water bath for 2 h, allows the oxidation into Fe_3O_4 to obtain cubic magnetite NPs (see Figure 5b).

The addition of compounds like dextran, polyvinyl alcohol (PVA), PAA, etc., in subsequent step of the reaction ensures protection of the magnetite cores from oxidation, increases biocompatibility and stabilizes the colloidal dispersion.

3.1.2. Thermal Decomposition

Thermal decomposition of organic iron precursor phase in presence of adequate surfactants (fatty acids, oleic acid (OA), oleylamine, etc.), driven in high temperatures, allows to improve the crystalline quality of iron oxide NPs with well controlled morphology, size and narrow distribution (see Figure 6). The reaction temperature is adjusted to the used solvents, which are usually compounds with high boiling points (octylamine, phenyl ether, phenol ether, hexadecanediol, octadecene, etc.).
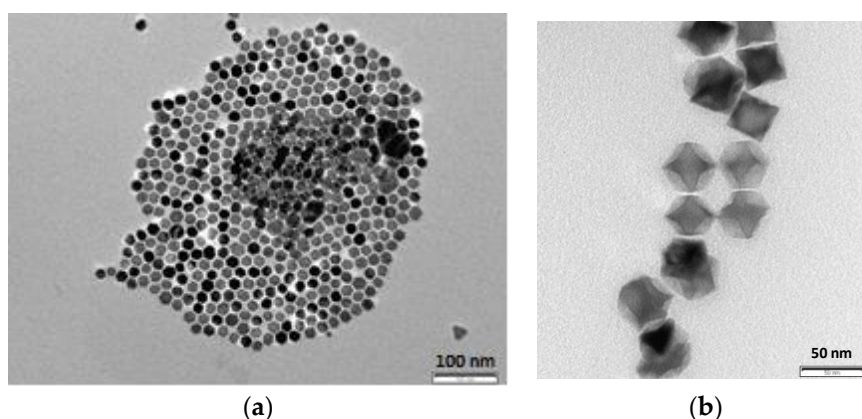

(**a**)　　　　　　　　　　　　　　(**b**)

Figure 6. TEM images of (**a**) hydrophobic Fe_3O_4@OA NPs and (**b**) hydrophobic cubic Fe_3O_4@OA NPs, obtained by thermal decomposition method.

The most commonly used iron organic precursors are iron(III) *N*-nitrosophenylhydroxylamine ($Fe(cup)_3$), iron(III) acetylacetonate ($Fe(acac)_5$), iron pentacarbonyl ($Fe(CO)_5$), which follow different routes: $Fe(cup)_3$ or $Fe(acac)_3$ directly decompose into magnetite/maghemite, while $Fe(CO)_5$ goes through an intermediate step of metal formation and then an oxidation of Fe^0 into magnetite by addition of a mild oxidant [36].

This procedure allows to obtain sophisticated hollow magnetite structures, which in the case of thermal decomposition of iron pentacarbonyl [37] produces in a first stage Fe@Fe_3O_4 structures (see Figure 7a) prior to the final formation of small hollow magnetite spheres (see Figure 6b). Large hollow magnetite spheres (see Figure 7c) can be obtained through the thermal decomposition of ferric chloride hexahydrate ($FeCl_3 \cdot 6H_2O$) [38].

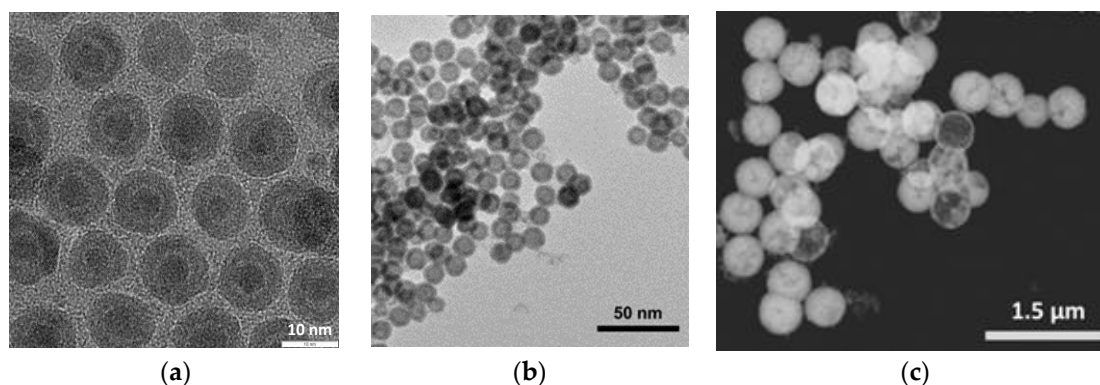**Figure 7.** TEM image of (**a**) Fe@Fe$_3$O$_4$@OA NPs 13 nm, (**b**) small hollow Fe$_3$O$_4$@OA NPs and (**c**) STEM of large hollow Fe$_3$O$_4$@OA NPs.

Thermal decomposition is a versatile procedure that allows also to obtain magnetite NPs with a diminished magnetic dead layer [39], different morphologies like spheres [40] or cubes [41], with narrow size distribution and controlled ion substitution with transition metals like Fe, Mn, Co, Ni, or Cr. However, the use on non-polar solvents is a main disadvantage that needs to be overcome by a phase transfer strategy, to change organic-stabilized NPs into water dispersions suitable for biomedical applications.

3.1.3. Hydrothermal Synthesis

Hydrothermal synthesis is a case of solvothermal procedures, that submit the reactants into a stainless-steel autoclave at high pressure and temperatures but using water as solvent. This high energy wet chemistry technique, produces NPs with high crystalline quality and optimum magnetic performances, since lattice formation benefits from the high temperatures (from 355 to 525 K), high vapor pressures (from 0.3 to 4 MPa) and long times (up to 72 h) to which the experimental conditions are subjected. Specifically, a combination of high temperatures, between 355 to 525 K, and prolonged reaction time (24 h), has been studied and successfully applied [42] to produce Fe$_3$O$_4$@OA (see Figure 8) and Fe$_3$O$_4$@PAA coated NPs, with sizes around 20 nm and high yield (nearly 86%), by mixing FeCl$_2$·4H$_2$O and FeCl$_3$·6H$_2$O in a Teflon vessel with either an OA or a PAA solution, respectively. The so obtained NPs show a high degree of crystallinity (see Figure 8) and a saturation magnetization (M$_S$ = 84 emu/g, close to the range of bulk magnetite (M$_S$~92 emu/g).
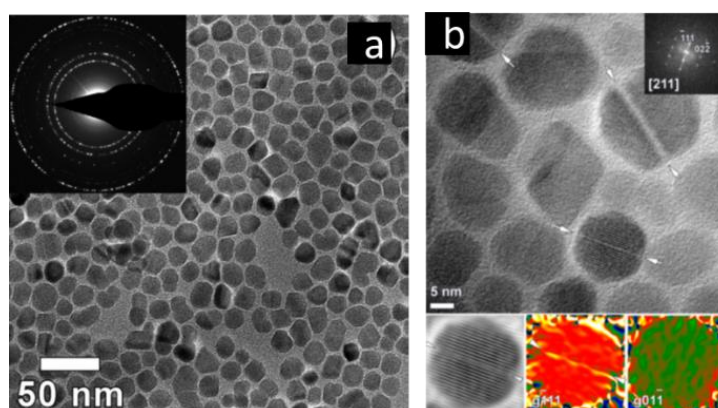

Figure 8. Fe$_3$O$_4$@OA coated NPs developed by hydrothermal method. (**a**) Low-resolution bright-field TEM images and corresponding ED ring patterns and (**b**) representative HRTEM image together with Fourier Transform FT pattern (inset). White arrows mark the dimer boundaries. Bottom insets: a filtered HRTEM image of a selected dimer NPs (**left**) and the corresponding GPA images for g1$\bar{1}$1 (**middle**) and g01$\bar{1}$ (**right**) diffraction spots. (Figures reprinted with permission from [42], ACS, 2014.

In another approach, magnetite NPs with rounded cubic shape and 39 nm were obtained by coprecipitation at 343 K of ferrous Fe^{2+} and ferric Fe^{3+} ions by $N(CH_3)_4OH$ solution, and a subsequent Teflon vessel thermal treatment at T = 523 K for 24 h [43]. The improved crystalline and magnetic quality after the annealing at high temperatures was clearly stated by the increase in M_S from 59.8 to 82.5 emu/g.

3.1.4. Solvothermal Procedures

Solvothermal procedures, using organic solvents at high pressure and temperature, open new possibilities to prepare magnetite NPs with complex configurations. Sphere like particles with an average size of 190 nm and containing multiple SPIONs cores closely packed inside a carbon coating shell were prepared using a mixture of ferrocene and acetone and kept at 513 K in a Teflon-lined stainless-steel autoclave for 72 h [44]. By means of chemical control, this solvothermal procedure is suitable to provide NPs with sizes between 100 and 250 nm [45] and morphologically controlled SPM multi-core $Fe_3O_4@C$ spheres (see Figure 9).

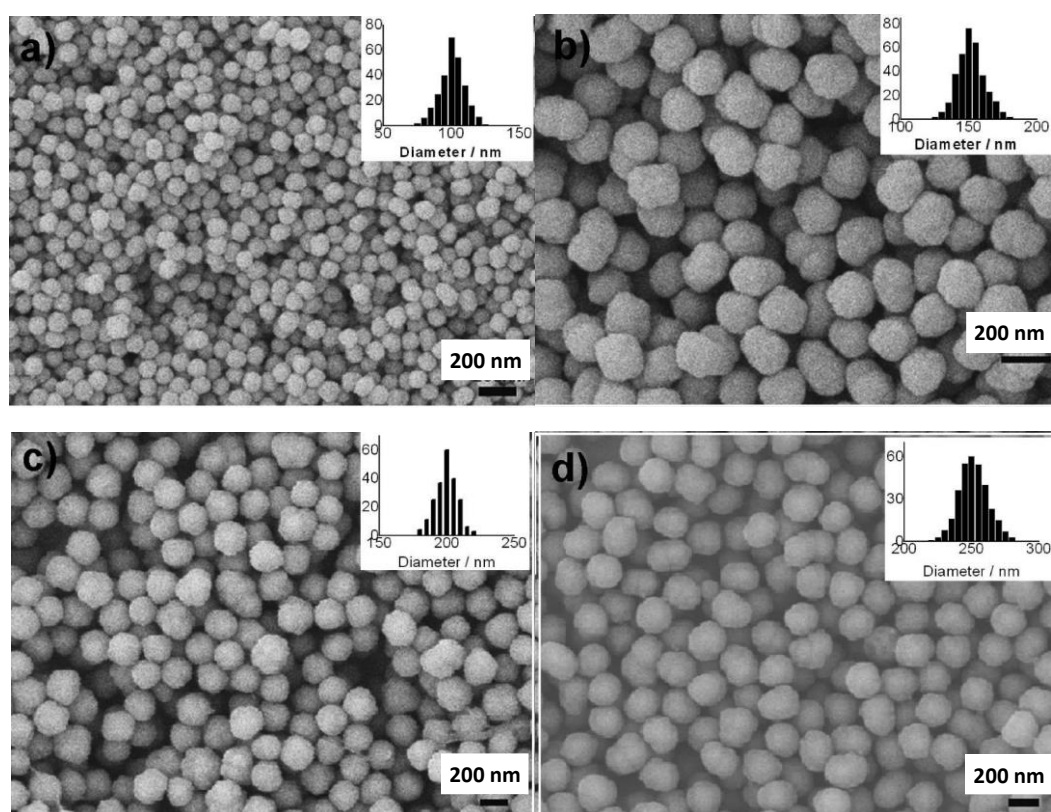**Figure 9.** SEM micrographs of SPM multi-core $Fe_3O_4@C$ spheres developed by a solvothermal technique with different amounts of hydrogen peroxide (**a**) 0.50, (**b**) 1.00, (**c**) 1.50, and (**d**) 2.00 mL, ensuring size control (**a**) 100, (**b**) 150, (**c**) 200, and (**d**) 250 nm. (Images reprinted with permission from [45], ACS, 2011).

3.1.5. Biogenic Inspired Procedures

Monodisperse magnetite NPs, with precise shape and size and crystalline quality, appear in magnetotatic bacteria, honeybees, pigeons, reptiles or amphibians. In humans, magnetite NPs can be found and are the signature of diseases in which an altered homeostasis of iron biomineralizes NPs at higher rates (neurological disorders, cancer, etc.). The mechanism of magnetite formation in living organisms (prokaryotes, archaea or eukaryotes) follows three steps: (1) formation of a specific organic reactor matrix (e.g., vesicles, protein cages, etc.) with favorable chemical environment; (2) formation of an intermediate iron compound and (3) conversion of this iron precursor into the magnetite NPs [46].

Compared to synthetic routes that occur at high energy operative conditions, natural magnetite biomineralization strategies occur at soft physiological conditions and are inspiring a new paradigm on green chemistry procedures. One of such strategies is based on the use of hollow Fn cages, an ubiquitous protein present in almost all living organisms that contains toxic Fe^{2+} and transforms it by oxidation into ferryhydrate (FeOOH)—an innocuous iron oxide mineral. In neurological diseases with a biologically altered iron homeostasis, the Fn protein shell transforms its ferryhydrate payload into magnetite NPs by a chemically complex procedure [47].

In a pioneering work [48], empty ferritin (apo-ferritin) was successfully used to synthesize magnetite NPs under high temperature and controlled pH conditions, opening a new bio-mimetic methodology based on the use of hollow biological cavities as templates to perform constrained reactions. Within this approach, cage like structures with sizes in the range from 18 to 500 nm, including virus capsids or ferritins obtained from different animal sources, have been used taking profit from their special characteristics (Fn from Pyrococcus furiosus remains stable above water boiling point) in synthetic procedures, at high reaction temperatures, to produce size controlled magnetite NPs [49,50].

3.2. Surface Functionalization: Core Protection, Colloidal Stability, Biocompatibility and Multifunctional Decoration

Physiological human media (blood, saliva, etc.) are a crowded biochemical environment with a complex machinery in which foreign materials (viruses, bacteria, etc.) are readily recognized and passivated by the immune system (IS) [51]. Therefore, nanoparticles exposed to in vitro or in vivo conditions require a highly engineered surface to protect the magnetite core from possible oxidation into hematite and ensure their magnetic quality, providing colloidal stability by preventing opsonization (unspecific attachment of a protein corona composed of albumin, immunoglobulin, apolipoproteins) [52] and providing abilities for theragnostic functions.

Different capping strategies include the use of small organic molecules, surfactants or active moieties like fluorescent molecules (rhodamine, fluorescein, etc.); natural polysaccharides, such as dextran, artificial block copolymers (poloxamers, poloxamines) or large polymers, like PEG that avoids opsonization [53]; inorganic materials, like amorphous or mesoporous silica and carbon, adding textural properties or thermal insulation; metal NPs (with plasmonic activity) and biological moieties for tagging, penetration or therapeutic abilities (monoclonal antibodies, aptamers, carbohydrates [53] and drugs).

3.2.1. Small Organic Molecules

Small organic molecules, or surfactants, can be anchored easily to magnetite NPs surface, since their hydroxyl groups, Fe-OH, greatly facilitate the anchoring of different compounds: alkoxylanes, carboxylic acids, phosphonic acids, dopamine, etc.

The most popular in situ coating consists in directly adding small biocompatible compounds (amino acid, citric acid, vitamin, cyclodextrin) during core synthesis.

However, additional enhancement of colloidal stability in basic or acidic media, where the organic molecules can decompose, can be achieved by grafting the Fe-OH group surface with silane groups, $Si-OCH_3$, which show good water stability and no cytotoxicity [54,55]. Different silane compounds are available, like 3-aminopropyltriethyloxysilane (APTES) and mercaptopropyltriethoxysilane (MPTES), providing chemical versatility [54] since they incorporate amino and sulfhydryl functional groups which facilitate bioconjugation procedures or drug grafting [55,56].

Phosphonic acid forms strong Fe-O-P bonds, which densely graft the magnetite NPs surface and allow a further combination with polydopamine groups, providing an improved pH and temperature stability [56]. Shahoo et al. have reported an efficient coating of 6–8 nm magnetite NPs, by oleic acid, lauric acid, phosphonic acids (dodecyl-; hexadecyl-) and dihexadecyl-phosphate, concluding that the bonding strengths of alkyl phosphonates and phosphates are stronger than that of carboxylate and proposed them as alternative biocompatible coatings in organic solutions [57].

Oleic acid ($CH_3(CH_2)_7CH = CH(CH_2)_7CO_2H$) provides large colloidal stability to magnetite NPs, but its lipophilic character is a main drawback in biomedical applications (see Figure 10). Its large steric stability, compared to similar compounds like stearic acid ($CH_3(CH_2)_{16}CO_2H$), arises from its cis-double-bond, which forms a kink in the middle of the carbon chain structure [58].
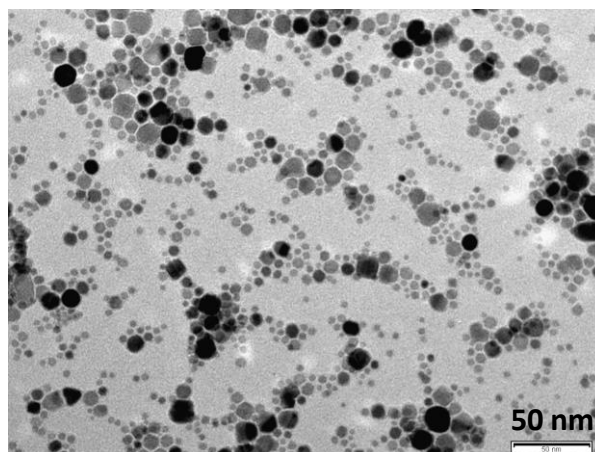

Figure 10. TEM images of magnetite NPs coated with oleic acid.

Moreover, reported by Guardia et al. [59], Fe_3O_4 NPs with sizes from 6 to 17 nm present large saturation magnetization values (M_S from 79 to 84 emu/g at T = 5 K), close to the bulk value (M_S = 92 emu/g), which in contrast to similar bare Fe_3O_4 NPs of 4 nm have only M_S = 50 emu/g. These results point to the role of oleic acid in reducing the spin surface disorder of small magnetite NPs, which is of large interest for the magnetic performance improvement in ultra-small SPIONs.

To enable lipophilic magnetite NPs [33] for biomedical applications which are mainly water based, a phase transfer, like the addition of amphiphilic molecules to the oil-soluble phase is the primary strategy to create a double layer with the hydrophilic segments exposed towards the solvent [60].

Additionally, surfactant exchange can be afforded by replacing the initial one by a new bifunctional surfactant, which has one group capable of binding to the NPs surface with a strong chemical bond and another terminal group that has a polar character and remains exposed to water [60].

Other interesting ability of organic coatings is the protection against degradation in acidic or basic media. Specifically, it has been reported [61] that magnetite coated with bipyridinium, F_3O_4@bipy NPs (13 nm) shows increased water solubility of the ferrofluid up to 300 mg/mL and stability of magnetite in a wide range of pH conditions, from very acidic to very basic ($1 \leq pH \leq 11$), extremely useful for acidic in vivo conditions like in tumor locations, where therapeutic procedures require an extended period of stability of Fe_3O_4 NPs.

3.2.2. Large Polymers

The incorporation of large polymers has been reported to add different advantages like size and shape control in one-pot procedures, enhanced colloidal stability, ability to prevent protein corona formation, biocompatibility and large availability of sites for the bioconjugation of biological moieties (aptamers, antibodies).

Their most remarkable fact is that they offer many repulsive groups balancing the attractive magnetic and Van der Waals interactions that agglomerate magnetite NPs and numerous sites for grafting antibodies, aptamers, etc. Synthetic functional polymers, such as linear or brush structures like, PEG, PVA, polylactic acid (PLA), polyvinilpirrolidone (PVP) or PAA, (see Figure 11) are commonly incorporated by two alternative approaches: grafting from and grafting onto the NPs.
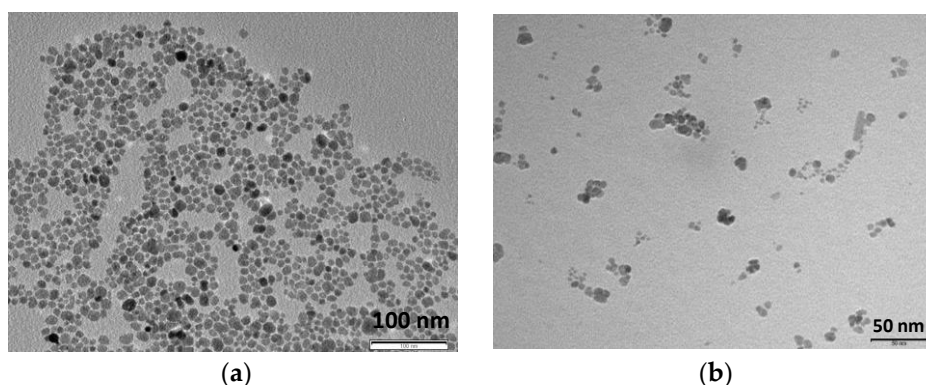
Figure 11. TEM images of magnetite NPs coated with (**a**) aminolauric acid and (**b**) polyacrylic acid (PAA).

Grafting polymers on the NPs' surface, by in situ procedures is the most used strategy, since it allows a strict control of the polymer's architecture and functionality, and although the density of grating is poor, the procedure is easier than a radical polymerization departing from monomer growth, which ensures a dense but uncontrolled coating.

In situ PAA grafting onto Fe_3O_4 NPs by a one-pot method has shown to produce materials with high colloidal stability and versatile surface for grafting biological molecules [62]. Other conventionally prepared one-pot polymer coated NPs include Fe_3O_4@PVP coated nanocrystals [63], with high colloidal stability in 10 different types of organic solvents and aqueous solutions, with pH ranging between 2.0 and 11.0. Generally, polyelectrolyte polymers provide enhanced colloidal stability when grafted onto magnetite NPs, owing to their electrostatic repulsive forces [64].

Other than stability, the incorporation of large polymers can be used to gain size and morphology control. In a one-pot procedure, by adding PVA to an aqueous solution of Fe^{2+}/Fe^{3+} salts with urea at 358 K, nanosized polyhedral particles with an approximated size around 300 nm and modified microspheres, between 100 to 280 nm, could be obtained controlling the polymer concentration [65]. A much more drastic effect on shape control has been shown when two PAA samples with average polymerization degrees of 208 and 126, PAA208 and PAA126, respectively, were used as an additive reactant to produce nanorods and flowerlike magnetite particles, respectively [65].

Besides enhancing colloidal stability, the specific interaction of the coating polymer with the physiological medium is of crucial importance in ensuring biocompatibility, facilitating bioconjugation or avoiding a fast entrapment by the IS. Therefore, taking inspiration from erythrocytes (red blood cells) whose chemical strategy to avoid protein corona formation comprises a protective shell barrier of hydrophilic oligosaccharide groups [66], a neutral electric surface composed of different hydrophilic coating shells (large brushes, densely packed [67]) have been synthetically incorporated and studied [68]. In this context, hydrophilic polymer brushes like linear dextrans and their derivatives, PEG; natural molecules, like polysialic acid, heparin, polysaccharides and artificial block-copolymers, like poloxamers or poloxamines, have shown to act as protein corona evaders [69].

From all these possibilities, PEG coating strategies, known as PEGylation, are the most used for biomedical applications, and their effectiveness in evading the IS depends on their molecular weight and density. PEGylated NPs with different molecules from 2000 and 20,000 g/mol and densities between 0.5 and 50 wt % have been shown to reduce opsonization from 1600 counts per million (cpm), to an almost constant value of 400 cpm, for PEG coating with MW larger than 5000 (g/mol), showing that PEGylation can hinder but not completely stop protein adsorption [67]. Coating density is a key factor in controlling the inter-distance between PEG terminal brushes that below a certain threshold hinder the adsorption of proteins. Above 5% of PEG coating, an inter-distance threshold about 1.0 nm between terminal PEG brushes can be estimated, and small protein adsorption remains constant below 400 cpm [67].

Functional polymers with responsive performance under pH, temperature or light irradiation stimuli are essential to provide controlled drug release [70]. Specifically, thermoresponsive polymer hydrogels like Pluronic, poly-isopropylacrilamide (PNIPAM) and their derivatives (e.g., PNIPAM with chitosan [71]) can be used to expel loaded molecules exploiting their coil-to-globule transition at defined temperatures. These hydrogels, in combination with SPIONs can be heated up by the application of an alternating magnetic field (magnetic hyperthermia) to undergo a controlled network shrinking useful for enhanced drug delivery applications [72].

3.2.3. Inorganic Materials

Inorganic materials are used also to confer core protection; colloidal stability and other functional properties like surface plasmon resonance (metal NPs), thermal isolation (carbon shell), etc. Silica (SiO_2) is one of the most commonly used inorganic coating materials, due to its versatile chemical silanol surface groups (-SiOH), colloidal stability and biocompatibility. The preparation of magnetite NPs coated with silica by sol-gel procedures allows to control the shell thickness [73] and is affordable by the basic hydrolysis of silanes in aqueous solutions of different organosilane compounds (tetraethyl orthosilicate (TEOS), APTES). The reaction between the oxide surface of magnetite and the silica takes places by the OH^- groups [74], and by an adjustment of the amount of added TEOS and the reaction time, the silica shell thickness can be easily tailored. Moreover, different configurations of the silica coated magnetite nanostructures can be achieved following two different routes: Stöber processes generally result into a multi-core coated NPs, while microemulsion processes provide mainly single core-shell NPs [74] (see Figure 12).
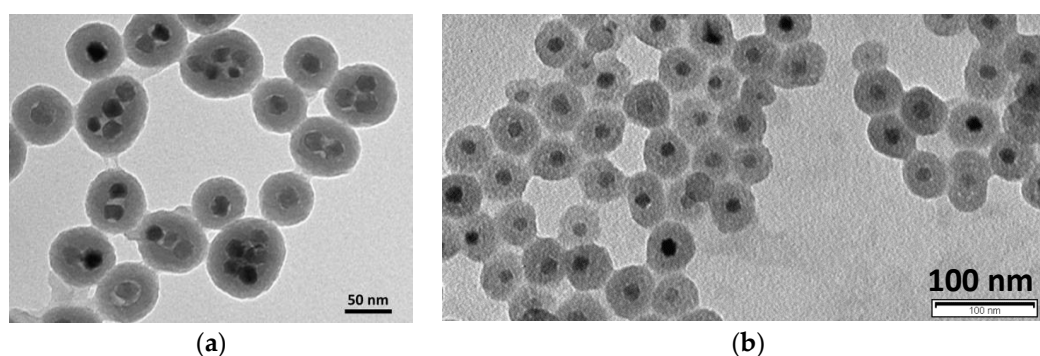

Figure 12. TEM micrographs of silica coated magnetite NPs by (**a**) Stöber processes, which generally result in multi-core coated NPs and (**b**) microemulsion processes, which provide mainly single core-shell NPs.

4. Biomedical Applications Arising from the Tunable Magnetic Properties of Magnetite Nanoparticles

The SPM character, inherent from the magnetite cores, allows to combine several abilities within a single nanostructure that can be triggered externally, under demand, by the application of a remote magnetic field to produce different magnetic responses of biomedical interest (summarized Table 2) like magnetophoresis, hyperthermia, magnetization or magnetic resonance.

Table 2. Summary of biomedical applications based on the combination of SPIONS and magnetic stimulation.

Magnetic Property	Application	Pros/Cons.	Commercial Kit	Toxicity
Magnetophoresis	Cell isolation	- Selective separation of tagged cells without damaging - Unaltered sample fluid after separation - Requires the use of antibodies for selective binding	MACS® Separators, Miltenyi	No in vitro toxicity
	Magnetofection	- Fast/efficient transfection of magnetized agents - Hallbach arrays with permanent magnets are cheap and easy to implement	NONE	No in vitro toxicity
	Magnetic guiding	- Magnetized stents can attract injected magnetic NPs to reduce restenosis - In preclinical stage	NONE	no in vivo toxicity tested in rat
Magnetic detection	Magnetometry SQUID	- Most sensitive magnetometry for iron detection - Expensive devices	NONE	No in vitro toxicity
	GMR sensors	- Detecting surface requires the binding of antibodies - Versatile for microarray detection	NONE	No in vitro toxicity
	Impedance Sensors	- Immunodetection requires the binding of antibodies - Implemented in paper strips kit - Attains detection limits in the clinical range	NONE	No in vitro toxicity
Inductive heating	Hyperthermia cancer treatment	- Selective killing of cancer cells - In clinical use for glioblastoma tumors - Increase of life expectancy 6–13 months	MAGFORCE NanoTherm, (clinical therapy)	NONE
	Thermally Enhanced release of therapeutic agents	- Controlled release by magnetic hyperthermia stimulation - Selective targeting - Under demand dosage - Under study stage	NONE	No in vitro toxicity
	Thermal stimulation	- Allows deep brain stimulation avoiding the implantation of electrodes in brain - In preclinical stage	NONE	no in vivo toxicity tested in mouse
Magneticre laxation	MRI contrast agents: single (T2)	- MRI contrast enhancement for soft tissues - In clinical use	Ferucarbotran (Resovist®, Bayer Healthcare) (MRI clinical diagnosis)	NONE
	MRI contrast agents: dual(T1/T2)	- Enhanced contrast for soft and hard tissues. - Avoiding the use of Gd for T1 contrast - In preclinical stage	NONE	no in vivo toxicity tested in mouse
Magnetic prototyping	3D magnetic bioprinting	- Bioprinting of tissue or replacements with biologically functional - No need of artificial substrate - Bioprinted functional saliva secretory organoids - Tested ex vivo - Under study stage	NONE	No in vitro and ex vivo toxicity

4.1. Magnetophoresis

Magnetophoresis refers to the controlled motion of SPIONs in a viscous medium induced by the application of an external magnetic field. This useful characteristic can be used to isolate, concentrate and drive magnetically labelled biomarkers or cells, from physiological samples (cerebrospinal fluid (CSF), blood, saliva, cell aspirates, etc.) and for in vivo targeting with the application of an external magnetic gradient. The use of magnetic separation techniques saves energy when exposing analytes to a permanent magnet and includes a high degree of specificity, if magnetic particles are conveniently

coated with antibodies that specifically target the desired biomarker. Moreover, extraction of the target can be done, without damaging the rest of the fluid for further analysis.

4.1.1. Cell Isolation

Purification and preconcentration of biomarkers or cells from patient's fluid samples or aspirates are crucial for a successful culture of isolated cells for transplantation or for an accurate high signal-to-noise ratio detection step (magnetic, optical or chemical) without the unspecific interference of other biochemical compounds in the sample [75]. Simple magnetic separation has been described by using cationic liposomes loaded with SPIONs (MCL), which were mixed with bone marrow aspirates under shaking for 1 h and transferred into tissue culture dishes, with a disk-shaped magnet at the bottom. Magnetically labeled cells were subject to the attraction of the magnetic field and 30% of them were isolated. Increased separation effectivity, up to an 85% was afterwards achieved using magneto-liposomes, conjugated with CD105 antibodies [76].

4.1.2. Magnetofection

Magnetofection, consists in the transfection of magnetic therapeutic vectors (plasmids, engineered viruses, etc.) inside cells, forced by a magnetic field, and is becoming a widely used technique in gene therapy which benefits from its higher degree of penetration compared to non-magnetic approaches.

Polyethylenimine-modified SPIONS/pDNA complexes (PEI-SPIONs/pDNA complexes) have been used to rapidly and uniformly distribute on the surface of MG-63 osteoblasts cells, by their incubation under the exposure to a uniform magnetic field enabled by specially designed Hallbach array of permanent magnets. With this homogeneous magnetic exposure, local transfection, without the disruption of the cells' membrane, was obtained, improving the magnetofection efficiency of pDNA into osteoblasts, thereby providing a novel approach for the targeted delivery of therapeutic genes to osteosarcoma tissues as well as a reference for the treatment of other tumors [77].

4.1.3. Magnetic Guiding

Magnetic guiding of MNPs exposed to the application of a magnetic gradient can be used to deliver therapeutic payloads in a precise location with a high degree of specificity. An innovative approach has been studied to reduce the re-stenosis of vasculature after stenting in in vivo experiments by combining stainless steel stents and the use of paclitaxel loaded SPIONs. The stents were magnetized upon the external application of a magnetic field, creating a magnetic field gradient capable to attract the MNPs delivered to the rat via a catheter. Paclitaxel release to the surrounding tissues was effective, reducing therefore restenosis of the vasculature tissue although the dose of paclitaxel-SPIONs was low [78].

4.2. Magnetic Detection

Magnetic detection exploits different aspects of the magnetic properties of both SPIONs and the components of the detecting sensors.

4.2.1. Superconducting Quantum Interference Device

(SQUID) is the most sensitive magnetometer for DC or low frequency measurements. Constituted by superconducting loops containing Josephson junctions, when a current is induced in the SQUID ring by an external magnetic flux, a change in voltage happens across the junction, which generates an output signal from the amplified voltage [79]. Although SQUID has been used to detect ferromagnetic contamination in the lungs or magnetite NPs brain in AD patients in ex vivo conditions [80], it has been applied to susceptibility measurements for in vivo identification of SPIONs loaded on a tumor in the lymph nodes of rats [81]. Moreover, the effectivity of iron quantification by SQUID magnetic relaxometry was successfully used to evaluate SPIONs conjugated to Her2-expressingMCF/Her2-18 cells (breast cancer cells) injected into xenograft MCF7/Her2-18 tumors in nude mice [82]. Brown

relaxation of magnetic NPs in liquids has also been exploited to detect biomarkers in liquid-phase immunoassays using SQUID magnetometry of magnetite beads conjugated with biotin, with sizes from 54 to 322 nm, attaining a sensitivity of 5.6×10^{-8} mol/mL [83].

4.2.2. Giant Magnetoresistance (GMR)

Giant Magnetoresistance (GMR) sensors are based on the significant change in electrical resistance of an arrangement of thin-film layers of alternating ferromagnetic and nonmagnetic conducting spacers when they are exposed to an externally applied magnetic field [84]. The variation in magnetoresistance of these spin-dependent sensors decorated with specific antibodies, provides quantitative analysis in combination with MNPs. The main strategy behind several magnetoresistive detectors, consists in attaching MNPs to the analytes, which during the detection procedure remain attached to the sensing surface creating a magnetic disturbance that triggers the change in electrical resistance of the device [85]. GMR detectors have been improved in the last years, being able to respond even upon small variations of magnetic fields, incrementing their sensitivity to detect small concentrations of analytes [84].

Although accurate GMR detection is facilitated by using SPM magnetite beads [86] with a large magnetic moment, a successful strategy using small SPIONs (30 nm) labeled with streptavidin was developed to detect Interleukin-6 (IL-6) antibody and amine modified DNA (deoxyribonucleic acid) oligonucleotide, by functionalizing the surface of the sensor with APTES and Glutathione [87]. This APTES-Glu modification was successfully extended to microarray detection, showing to be a versatile and robust method [87].

4.2.3. Impedance Based Sensor

Emergent strategies are trying to couple lateral flow immunoassay (LFIA) (paper-strips), which stand out for their low-cost, speed, portability and ease of use, with an innovative magnetic detection based on Cu-impedance change in the presence of MNPs [88].

The sensing property relies on the high rate of oscillation of the magnetic moments of the SPIONs that induces localized eddy currents on the surface of the sensor, increasing its electrical radio-frequency impedance, for which no external magnetic field is required. This facile magnetic detection strategy is based on the use of paper-strip immunodetection kits in combination with SPIONS functionalized to specifically bind to prostate-specific antigen PSA. The strips were seeded with capture anti-PSA antibody and anti-IgG (both at a concentration of 1 mg/mL) forming the test and control lines, respectively. PSA standard solutions at known concentrations were submitted to the strip and attached to test line. The subsequent binding of conjugated SPIONs to PSA ensured the magnetic reading and the final determination of analyte concentrations. This facile method allowed to attain a limit of detection within the clinical range of interest around 0.25 ng/mL and a resolution of 50 pg [89].

Further improvements are reported, by using large SPM multi-core carbon coated nanoflowers (Fe_3O_4@C) as LFIA labels that provide a magnetic moment substantially larger than that of single-core SPIONs, allowing for a more sensitive and precise detection [90].

4.3. Inductive Heating

Inductive heating, also known as magnetic hyperthermia, consists in the transformation of electromagnetic energy into heat, when an alternating external magnetic field (f = 3 kHz, 300 MHz) is applied to a magnetic nanoparticle. The temperature rise that is transmitted to the medium, in which the NPs are housed, depends on the magnetic quality of the NPs, the viscosity of the medium and the parameters of the external magnetic field, among others [91]. This externally controlled rise of temperature can be used for killing cancer cells when rising to 315 K, stimulating cell growth for mild thermal increase or triggering release mechanisms for enhanced delivery.

4.3.1. Cancer Hyperthermia Treatment

Through magnetic hyperthermia, cancer treatments can be developed by selectively heating between 314 and 316 K cancerous tissues which are previously loaded with MNPs. In biomedical applications, magnetic exciters are restricted to a safety upper limit of $H \cdot f < 4.58 \times 10^8$ A·m·s^{-1} [92].

This technique benefits from a natural mechanism called enhanced permeation and retention, due to the defects and poor drainage of cancerous tissues that cause the accumulation of NPs inside the damaged tissue [93]. This entrapment of NPs inside the tumor tissue allows the heating and weakening of cancer cells, minimizing side effects in the surrounding healthy cells. It is worth highlighting the development by MagForce [94] of a clinically used magnetic hyperthermia therapy, which combines a magnetic field applicator (100 kHz) and an injectable therapeutic agent consisting in Fe_3O_4@amylosan NPs to treat glioblastoma, an aggressive brain tumor.

Within this commercial solution, even large tumors around 5 cm can be treated by the direct injection with 3 mL of magnetite based ferrofluid, which heats up by the application of the external alternating magnetic fields. This technique has been used in phase II clinical trials in combination with stereotactic radiotherapy and obtained the European approval as a treatment for brain tumors in 2010, after demonstrating its ability to increase life expectancy from 6 to 13 months in patients with glioblastoma multiforme, compared to others treated only with chemotherapy.

4.3.2. Controlled Release

Another therapeutic strategy based on magnetic hyperthermia consists in the thermal stimulation of thermo-active moieties to provoke the release of therapeutic agents (drugs, growth factor, oligomers, etc.) under demand.

One of the most successful drug delivery applications, triggered by magnetic hyperthermia, combines SPIONs with a coating of thermosensitive polymers such as PNIPAM and its derivates. These polymers form hydrogels at room temperature and can allocate molecules acting as drug nanocarriers. When the temperature rises above a critical range (T = 306–313 K), these structures retract and expel all the drug contained within.

Steps are being taken so that this technique meets the essential conditions of an effective tool in precision medicine, temperature control and release time control. In fact, it has already been possible to produce the collapse of 49% of the volume of the therapeutic agent at a temperature of biomedical interest T = 311 K (see Figure 13) [95]. Optimizing the biopolymers mixture (PNIPAM/chitosan), it is even possible to release 70% of the drug housed in a single second [71].
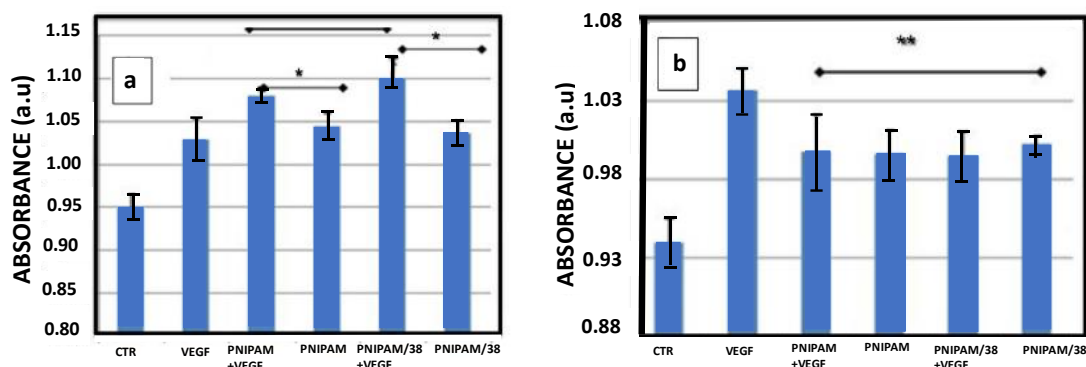

Figure 13. Absorbance measurements performed to address VEGF release for HUVEC cells incubated with PNIPAM (release temperature at 305 K) and PNIPAM/38 (release temperature at 311 K) loaded with VEGF and raised to different temperatures, (**a**) 311 K and (**b**) 293 K. The wells with standard cultural medium with and without VEGF (10 ng/mL) were used as controls. Experiments performed at 311 K show the ability of thermal release of VEGF loaded on PNIPAM based materials. (Images reprinted with permission from [95], Springer, 2014).

Besides drugs, there is a large interest in the controlled release of biological moieties with therapeutic effects for regenerative medicine. Several proteins (recombinant human bone morphogenic proteins, rhBMPs, induce osteogenesis) and growth factors (vascular endothelial growth factor (VEGF)) responsible for the triggering of angiogenesis (process of blood vessel formation) are crucial for ensuring the long-term viability of repaired tissues with functional recovery. Specifically, VEGF is effective only when concentration gradients at physiological levels are generated, and new strategies are needed for an adequate delivery at the site of tissue repair. In this context, the grafting complex-elastin-dendron-VEGF hyperbranched poly(epsilon-lysine) peptides integrating in their core parallel thermoresponsive elastin-like peptide sequences over the surface of Fe_3O_4@PAA NPs (see Figure 14) has been reported [96].
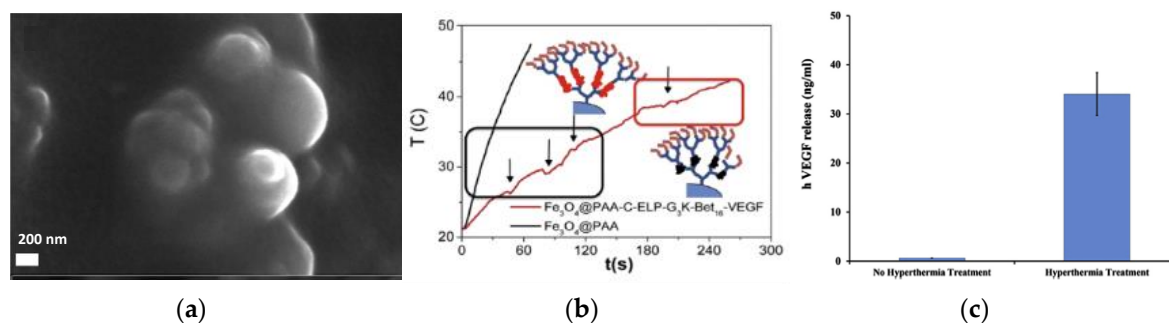

(a)   (b)   (c)

Figure 14. (**a**) SEM micrograph of Fe3O4@PAA-C-ELP-G3K-Bet16-VEGF, (**b**) hyperthermia Treatment of Fe_3O_4@PAA and Fe_3O_4@PAA-C-ELP-G3K-Bet16 samples immersed in phosphate buffered saline, pH 7.4, with a volume of 240 μL and a magnetite concentration of 40 μg/μL, and (**c**) release of hVEGF from Fe_3O_4@PAA-C-ELP-G3K-Bet16-VEGF after hyperthermia treatment. Negative control shows no hVEGF release after hyperthermia treatment. (Images taken form [96], Elsevier, 2015).

These functionalized SPIONs were able to avidly bind VEGF forming a stable complex. Under the adequate stimulation of the complex Fe_3O_4@PAA-C-ELP-G3K-Bet16-VEGF with a magnetic induction (H = 30 mT, f = 298 kHz), a mild-temperature rise up to 315 K, the range at which the elastin-like peptides collapse provoked the VEGF release in only two minutes after magnetic stimulation without suffering degradation (see Figure 14).

4.3.3. Thermal Stimulation

Additionally, it is worth mentioning a last application of magnetic hyperthermia that has been able to produce DBS (Deep brain stimulation) at the nanometric level in a mouse with induced thermal sensitivity in specific neurons selected by genetic technique. The mouse brain was injected with SPIONs (around 22 nm) and exposed to an external magnetic field which provoked a local increase in temperature. With this procedure, the selective activation of the modified neurons was observed, without any secondary effect in the neighboring neurons, which were preserved practically intact [97].

In another recent study [98], the effect of magnetoelectric particles has been modeled to stimulate the brain of an affected Parkinson's patient by simulating a neural network with electrical levels like those of a healthy person. The simulation estimates optimal values for the design made from 20 nm magnetite NPs, with a concentration of 3×10^6 under the action of an external magnetic field of 300 Oe operating at a frequency 80 Hz. Undoubtedly, these results open the door to the effective development of new innovative and non-invasive DBS methodologies.

4.4. Magnetic Resonance Imaging

Nuclear magnetic resonance (NMR) is a powerful magnetic phenomenon mainly used in clinics for imaging. In contrast to a surface-based sensor like GMR, NMR is capable of sampling an entire volume in a non-invasive way. MRI can be combined with other diagnostic tools, like CT (X-ray computed tomography), PET (positron emission tomography) or US (ultrasound), to obtain more

accurate diagnosis, for which multimodal SPIONs can be afforded either combining several agents into a single carrier or by engineering a material which can be active in several modalities [99].

It is a known fact that the magnetic core creates a local magnetic inhomogeneity, which alters the relaxation time of hydrogen protons in the surrounding water molecules. This fact has motivated different studies based on the use of magnetic NPs as dual MRI contrast agents for T1 and T2 relaxation, in order to avoid the conventionally used gadolinium chelates and their potential toxicity.

The strategies developed so far to optimize the magnetic response of magnetite based NPs as MRI contrast agents have been focused in tailoring their architecture: large particles containing several SPM single cores (magnetic beads), hollow magnetite spheres and single core NPs of pure magnetite or doped with transition metals [100].

SPM beads, composed of dozens of SPIONs within a carbon shell [25] and with an approximate diameter around 100 nm (see Figure 15), have been shown to present a large relaxivity ($r_2 = 218$ mM^{-1} s^{-1}) combined with a negligible thermal rise when tested in magnetic hyperthermia tests (H = 30 mT, f = 293 kHz).
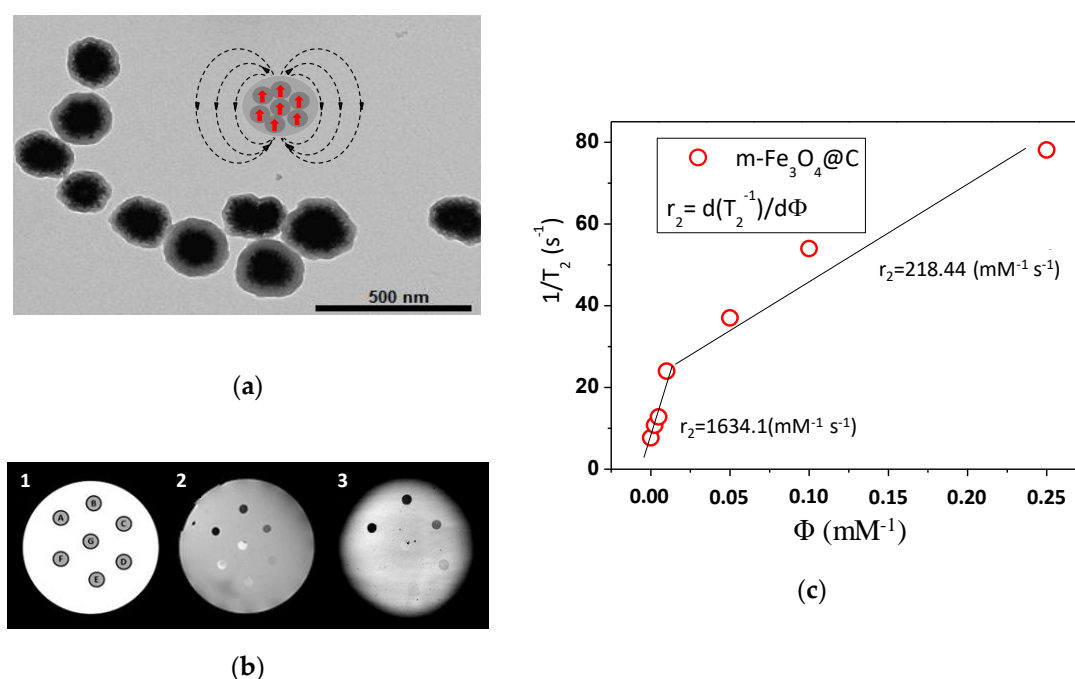

Figure 15. (**a**) TEM image of multi-Fe$_3$O$_4$@C NPs, (**b**) scheme of the phantom NPs concentration distribution (b.1): A = 0.25 mg/mL; B = 0.1 mg/mL; C = 0.05 mg/mL; D = 0.025 mg/mL; E = 0.005 mg/mL; F = 0.0025 mg/mL and G = 0 mg/mL; MR T2-weighted image of the agar phantom (b.2); MR T2*-weighted image of the agar phantom (b.2), performed at 9.4 T (BrukerBiospec) on a set of agar phantoms loaded with different concentrations of NPs (0.0025 to 0.25 mM) and (**c**) relaxivity calculated from T2 MRI relaxation on agar phantoms reprinted with permission from [25], IEEE, 2016.

This combination of enhanced MRI contrast and poor thermomagnetic response offers a potential advantage for using these materials in therapeutic situations, like brain applications, where any temperature increase is highly inadvisable for patients [101]. In this case, despite the high content of magnetic material content in the NPs, the carbon coating shell plays the fundamental role of thermal insulation, which decouples the magnetic activity of the NPs from its thermal response.

Further enhancement of MRI contrast has been achieved by exploring the effect of shape on T2 relaxation mechanisms, using single core magnetite NPs. In this context, water-dispersible polyethylene glycol-phospholipid (PEGphospholipid) coated cubic SIONPs (see Figure 16) showed extremely high r_2 relaxivity (up to 761 mM^{-1} s^{-1}) [102], yielding superior in vivo MRI details. Ascribing this exceptionally high relaxivity to the magnetic shape anisotropy, magnetite NPs with different shapes were studied,

from octapod (D = 30 nm, r_2 = 679.3 ± 30 mM^{-1} s^{-1}) [103] to rod-like length of 30–70 nm and diameter of 4–12 nm, seeming to confirm this hypothesis.

(**a**)	(**b**)

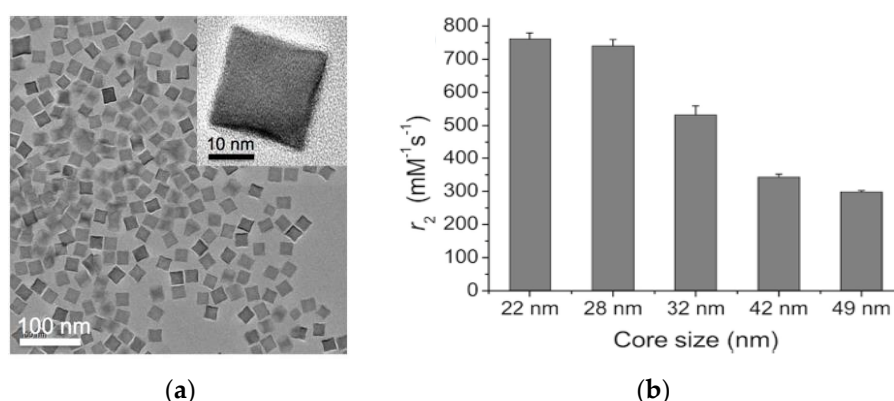**Figure 16.** (**a**) TEM image of coated cubic SPIONs and (**b**) size dependent r2 relaxivity, reprinted with permission from [102] (ACS, 2012).

Gadolinium, a paramagnetic ion with the largest number of unpaired electrons, is the most effective T1 contrast agent, which has however the main drawback of being toxic. Although it is always used in combination with chelating molecules with the aim of avoiding its potential risk, alternative strategies are seeking to exploit new aspects of SPIONs to produce versatile dual contrast agents, taking advantage of the existing SPION (Ferucarbotran (Resovist®), Bayer Healthcare) clinically approved as MRI contrast agent. Ultra-small magnetite NPs with a diameter around 3.5 nm have been studied as candidates for dual-modal MRI contrast with simultaneous T1/T2 switching, activity [104]. In this study, the observed switching between T1–T2 contrast (see Figure 17) is ascribed to the fact that ultra-small SPIONs are single-dispersed in blood and produce T1 contrast, while after their extravasation and accumulation in the tumoral site, the NPs' self-assembling into larger clusters induces the appearances of T2 contrast modulated by magnetic interactions.
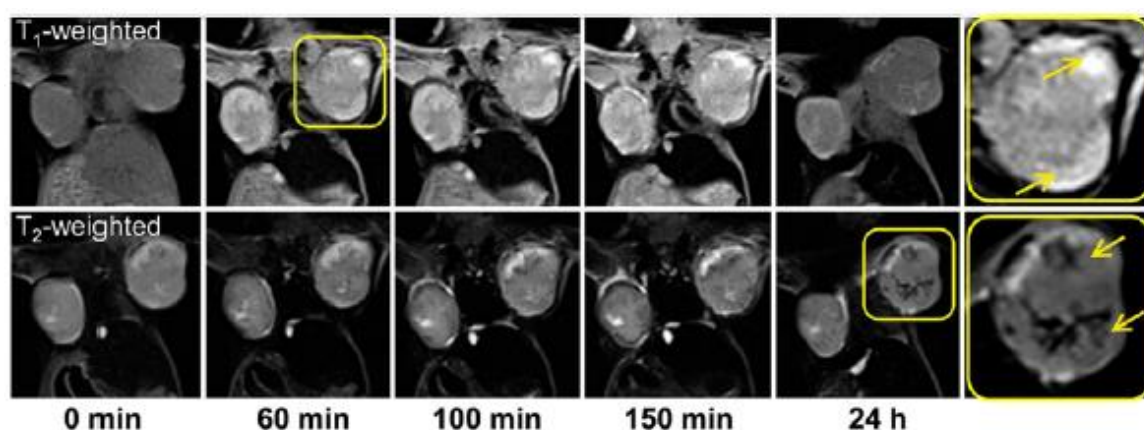

Figure 17. T1- and T2-weighted MRI of a mouse bearing orthotopic 4T1 tumors before and after i.v. administration of ultra-small SPIONs at different time points. Bright contrast with increasing signal in T1-weighted MR images was observed in the tumor, particularly peripheral regions (inset), at early time points (i.e., 5–150 min) resulting from the single-dispersed ultra-small SPIONs, whereas signals in several regions of the tumor turning dark (arrow indicated) were observed in T2-weighted images 24 h after ultra-small SPIONs injection because of ultra-small SPIONs clustering in the tumor interstitials. (Image reprinted with permission from [104], ACS, 2017).

4.5. Magnetic Prototyping of Functional Biological Structures

One of the milestones in regenerative medicine is the fabrication of tissue, replacements or organs with biologically relevant functionality. This emerging field combines multiple strategies arising from different approaches like cell-based therapies, tissue-engineered biomaterials, scaffolds or implantable devices. The exposure of magnetized cells under a three-dimensional (3D) magnetic pattern, known as 3D magnetic bioprinting, allows the prototyping of organelles or autologous implantable biodevices without the need of a material substrate.

Recently a 3D bio-fabrication system, by magnetic 3D bioprinting (M3DB), has been tested to generate innervated saliva secretory (SG) organoids using magnetized neural crest derived mesenchymal stem cells (human dental pulp stem cells (hDPSC). The magnetized cells were spatially arranged with magnet dots to generate 3D spheroids and afterwards cultured with fibroblast growth factor 10 to promote epithelial morphogenesis and neurogenesis. The preformed SG organoids were then transplanted into ex vivo model showing epithelial growth, innervation and production of salivary a-amylase upon FGF10 stimulation [105].

5. Conclusions

Magnetite NPs with superparamagnetic behavior, commonly known as SPIONS, can be easily tailored in nanostructured materials combining functional organic or inorganic matrices (mesoporous or amorphous silica, biocompatible polymers like chitosan, k-carragenan, PNIPAM, PEG, PAA) to incorporate therapeutic or tagging moieties like drugs, aptamers or antibodies.

The list of nanostructured materials containing magnetite NPs is immense, and the applications in nanomedicine cover almost any aspect from diagnosis, therapy or regenerative medicine, since in all cases the nanostructure inherits the intrinsic properties of magnetite that ensure multiple abilities like magnetic separation/detection/targeting, magnetofection, magnetic resonance contrast imaging, magnetic hyperthermia therapy and stimulated delivery, magnetic cell growth stimulation and 3D magnetic prototyping of organelles.

References

1.	Jacobs, I.S. Role of Magnetism in Technology. *J. Appl. Phys.* **1969**, *40*, 917. [CrossRef]

2.	Jacobs, S.; Bean, C.P. Fine Particles, Thin Films and Exchange Anisotropy. In *Magnetism*; Rado, G.T., Suhl, H., Eds.; Academic: New York, NY, USA, 1963; Volume 3, pp. 271–350.

3.	Guéron, S.; Deshmukh, M.M.; Myers, E.B.; Ralph, D.C. Tunneling via Individual Electronic States in Ferromagnetic Nanoparticles. *Phys. Rev. Lett.* **1999**, *83*, 4148–4151. [CrossRef]

4.	Liou, S.H.; Huang, S.; Klimek, E.; Kirby, R.D.; Yao, Y.D. Enhancement of coercivity in nanometer-size CoPt crystallites. *J. Appl. Phys.* **1999**, *85*, 4334–4336. [CrossRef]

5.	Sridhar, S.; Amiji, M.; Shenoy, D.; Nagesha, D.; Weissig, V.; Fu, W. Nanomedicine: A new paradigm in diagnosis and therapy. *Optics East 2005* **2005**, *6008*, 600816. [CrossRef]

6.	Piñeiro, Y.; Vargas, Z.; Rivas, J.; López-Quintela, M.A. Iron Oxide based Nanoparticles for Magnetic Hyperthermia Strategies in Biomedical Applications. *Eur. J. Inorg. Chem.* **2015**, *27*, 4495–4509. [CrossRef]

7.	Dobson, J. Nanoscale biogenic iron oxides and neurodegenerative disease. *FEBS Lett.* **2001**, *496*, 1–5. [CrossRef]

8. Ramos-Cabrer, P.; Campos, F. Liposomes and nanotechnology in drug development: Focus on neurological targets. *Int. J. Nanomed.* **2013**, *8*, 951–960. [CrossRef]

9. Anselmo, A.C.; Mitragotri, S. Nanoparticles in the clinic. *Bioeng. Transl. Med.* **2016**, *1*, 10–29. [CrossRef]

10. Xiang, Y.; Wang, J. Current status of superparamagnetic iron oxide contrast agents for liver magnetic resonance imaging. *World J. Gastroenterol.* **2015**, *21*, 13400–13402.

11. NanoTherm. Available online: https://www.magforce.com/en/home/our_therapy/ (accessed on 28 July 2019).

12. Vallabani, N.V.S.; Singh, S. Recent advances and future prospects of iron oxide nanoparticles in biomedicine and diagnostics. *Biotech* **2018**, *8*, 279. [CrossRef]

13. Ortolani, A.; Bianchi, M.; Mosca, M.; Caravelli, S.; Fuiano, M.; Marcacci, M.; Russo, A. The prospective opportunities offered by magnetic scaffolds for bone tissue engineering: A review. *Joints* **2016**, *4*, 228–235. [CrossRef] [PubMed]

14. Cornell, R.M.; Schwertmann, U. *The Iron Oxides: Structure, Properties, Reactions, Occurences and Uses*, 2nd ed.; Wiley-VCH: Wienheim, Germany, 2003.

15. Banerjee, S.K.; Moskowitz, B.M. *Magnetite Biomineralization and Magnetoreception in Organisms, a New Biomagnetism*; Kirschvink, J.L., Jones, D.S., MacFadden, B.J., Eds.; Chapter 2: Ferrimagnetic Properties of Magnetite; Springer: New York, NY, USA, 1985.

16. Parkinson, G.S. Iron Oxide Surfaces. *Surface Sci. Rep.* **2016**, *71*, 272–365. [CrossRef]

17. Verwey, E.J.W. Electronic Conduction of Magnetite (Fe_3O_4) and Its Transition Point at Low Temperatures. *Nature* **1939**, *144*, 327–328. [CrossRef]

18. Senn, M.S.; Wright, J.P.; Attfield, J.P. Charge Order and Three-Site Distortions in the Verwey Structure of Magnetite. *Nature* **2012**, *481*, 173–176. [CrossRef]

19. Goodenough, J.B. *Magnetism and the Chemical Bond*; Wiley-Interscience: New York, NY, USA, 1963.

20. Skomski, R.; Sellmeyer, D. *Cap.1, Handbook of Advanced Magnetic Materials*; Sellmeyer, D.J., Liu, Y., Shindo, D., Eds.; Tingshua University Press: New York, NY, USA, 2006.

21. Landau, L.D.; Lifshitz, E. On the theory of the dispersion of magnetic permeability in ferromagnetic bodies. *Phys. Z. Sowjetunion* **1935**, *8*, 153–169.

22. Blundell, S. *Magnetism in Condensed Matter*; Oxford University Press: New York, NY, USA, 2001.

23. Krishnan, K.M. Biomedical Nanomagnetics: A Spin Through Possibilities in Imaging, Diagnostics, and Therapy. *IEEE Trans. Magn.* **2010**, *46*, 2523.

24. Yoon, K.Y.; Xue, Z.; Fei, Y.; Lee, J.H.; Cheng, V.; Bagaria, H.G.; Huh, C.; Bryant, S.L.; Kong, S.D.; Ngo, V.W.; et al. Control of magnetite primary particlesize in aqueous dispersions of nanoclusters for high magnetic susceptibilities. *J. Colloid Interface Sci.* **2015**, *462*, 359–367. [CrossRef]

25. Vargas-Osorio, Z.; Argibay, B.; Piñeiro, Y.; Vázquez-Vázquez, C.; López-Quintela, M.A.; Álvarez-Pérez, M.A.; Sobrino, T.; Campos, F.; Castillo, J.; Rivas, J. Multicore Magnetic Fe3O4@C Beads with Enhanced Magnetic Response for MRI in Brain Biomedical Applications. *IEEE Trans. Magn.* **2016**, *52*, 230604. [CrossRef]

26. Cótica, L.F.; Santos, I.A.; Girotto, E.M.; Ferri, E.V.; Coelho, A.A. Surface spin disorder effects in magnetite and poly(thiophene)-coated magnetite nanoparticles. *J. Appl. Phys.* **2010**, *108*, 064325. [CrossRef]

27. Nedelkoski, Z.; Kepaptsoglou, D.; Lari, L.; Wen, T.; Booth, R.A.; Oberdick, S.D.; Galindo, L.; Ramasse, Q.M.; Evans, R.F.L.; Majetich, S.; et al. Origin of reduced magnetization and domain formation in small magnetite nanoparticles. *Sci. Rep.* **2017**, *7*, 45997. [CrossRef]

28. Fiorani, D. *Surface Effects in Magnetic Nanoparticles*; Fiorani, D., Ed.; Springer: New York, NY, USA, 2005.

29. Lacroix, L.-M.; Lachaize, S.; Falqui, A.; Blon, T.; Carrey, J.; Dumestre, F.; Amiens, C.; Margeat, O.; Chaudret, B.; Lecante, P.; et al. Ultrasmall iron nanoparticles: Effect of size reduction on anisotropy and magnetization. *J. Appl. Phys.* **2008**, *103*, 7. [CrossRef]

30. Park, J.; An, K.J.; Hwang, Y.S.; Park, J.G.; Noh, H.J.; Kim, J.Y.; Park, J.H.; Hwang, N.M.; Hyeon, T. Ultra-large-scale syntheses of monodisperse nanocrystals. *Nat. Mater.* **2004**, *3*, 891–895. [CrossRef] [PubMed]

31. Guardia, P.; Labarta, A.; Batlle, X. Tuning the Size, the Shape, and the Magnetic Properties of Iron Oxide Nanoparticles. *J. Phys. Chem. C* **2011**, *115*, 390–396. [CrossRef]

32. Verma, J.; Lal, S.; van Noorden, C.J.F. Nanoparticles for hyperthermic therapy synthesis strategies and applications in glioblastoma. *Int. J. Nanomed.* **2014**, *9*, 2863–2877.

33. Bañobre-López, M.; Piñeiro Redondo, Y.; López-Quintela, M.A.; Rivas, J. *Handbook of Nanomaterials Properties*; Bhushan, B., Luo, D., Schricker, S., Sigmund, W., Zauscher, S., Eds.; Chapter 15: Magnetic Nanoparticles for Biomedical Applications; Springer-Verlag: Berlin, Germany, 2014.

34. La Mer, V.K.; Dinegar, R.H. Theory, production and mechanism of formation of monodispersed hydrosols. *J. Am. Chem. Soc.* **1950**, *72*, 4847–4854. [CrossRef]

35. Sugimoto, T.; Matijevic, E.J. Formation of uniform spherical magnetite particles by crystallization from ferrous hydroxide gels. *Colloid Interface Sci.* **1980**, *74*, 227–243. [CrossRef]

36. Hyeon, T.; Lee, S.S.; Park, J.; Chung, Y.; Na, H.B. Synthesis of highly crystalline and monodisperse maghemite nanocrystallites without a size-selection process. *J. Am. Chem. Soc.* **2001**, *123*, 12798–12801. [CrossRef]

37. Peng, S.; Sun, S. Synthesis and Characterization of Monodisperse Hollow Fe$_3$O$_4$ Nanoparticles. *Angew. Chem.* **2007**, *119*, 4233–4236. [CrossRef]

38. Xiaohui, L.; Guangbin, J.; Yousong, L.; Huang, O.; Yang, Z.; Du, Y. Formation mechanism and magnetic properties of hollow Fe3O4 nanospheres synthesized without any surfactant. *Cryst. Eng. Comm.* **2012**, *14*, 8658–8663.

39. Unni, M.; Uhl, A.M.; Savliwala, S.; Savitzky, B.H.; Dhavalikar, R.; Garraud, N.; Arnold, D.P.; Kourkoutis, L.F.; Andrew, J.S.; Rinaldi, C. Thermal Decomposition Synthesis of Iron Oxide Nanoparticles with Diminished Magnetic Dead Layer by Controlled Addition of Oxygen. *ACS Nano* **2017**, *11*, 2284–2303. [CrossRef]

40. Tong, S.; Quinto, C.A.; Zhang, L.; Mohindra, P.; Bao, G. Size-Dependent Heating of Magnetic Iron Oxide Nanoparticles. *ACS Nano* **2017**, *11*, 6808–6816. [CrossRef] [PubMed]

41. Dokyoon, K.; Nohyun, L.; Mihyun, P.B.; Hyo, K.K.; An Taeghwan, H. Synthesis of Uniform Ferrimagnetic Magnetite Nanocubes. *J. Am. Chem. Soc.* **2009**, *131*, 454–455.

42. Kolen'ko, Y.; Bañobre-López, M.; Rodriguez-Abreu, C.; Carbo-Argibay, E.; Sailsman, A.; Piñeiro-Redondo, Y.; Cerqueira, M.F.; Petrovykh, D.; Kovnir, K.; Lebedev, O.; et al. Large-Scale Synthesis of Colloidal Fe$_3$O$_4$ Nanoparticles Exhibiting High Heating Efficiency in Magnetic Hyperthermia. *J. Phys. Chem. C* **2014**, *118*, 8691–8701. [CrossRef]

43. Daou, T.J.; Pourroy, G.; Begin-Colin, S.; Greneche, J.-M.; Ulhaq-Bouillet, C.; Légaré, P.; Bernhardt, P.; Leuvrey, C.; Rogez, G. Hydrothermal Synthesis of Monodisperse Magnetite Nanoparticles. *Chem. Mater.* **2006**, *18*, 4399–4404. [CrossRef]

44. Wang, H.; Sun, Y.B.; Chen, Q.W.; Yu, Y.F.; Cheng, K. Synthesis of carbon-encapsulated superparamagnetic colloidal nanoparticles with magnetic-responsive photonic crystal property. *Dalton Trans.* **2010**, *39*, 9565–9569. [CrossRef]

45. Wang, H.; Chen, Q.W.; Yu, Y.F.; Cheng, K.; Sun, Y.B. Size- and solvent-dependent magnetically responsive optical diffraction of carbon encapsulated superparamagnetic colloidal photonic crystals. *J. Phys. Chem. C* **2011**, *115*, 11427–11434. [CrossRef]

46. Gorobets, O.; Gorobets, S.; Koralewski, M. Physiological origin of biogenic magnetic nanoparticles in health and disease: From bacteria to humans. *Int. J. Nanomed.* **2017**, *12*, 4371–4395. [CrossRef]

47. Uchida, L.; Liepold, O.; Douglas, T. *Protein Cage Magnetic Nanoparticles in Magnetic Nanoparticles from Fabrication to Clinical Applications*; Thanh, N.T.K., Ed.; Taylor and Francis: Boca Raton, FL, USA, 2012; pp. 73–95.

48. Meldrun, F.C.; Wade, V.J.; Nimmo, D.L.; Heywood, B.R.; Mann, S. Synthesis of inorganic nanophase materials in supramolecular protein cages. *Nature* **1991**, *349*, 684–687. [CrossRef]

49. Fantechi, E.; Innocenti, C.; Zanardelli, M.; Fittipaldi, M.; Falvo, E.; Carbo, M.; Shullani, V.; Manelli, C.; Ghelardini, C.; Ferret, A.M.; et al. A smart platform for hyperthermia application in cancer treatment: Cobalt-doped ferrite nanoparticles mineralized in human ferritin cages. *ACS Nano* **2014**, *8*, 4705–4719. [CrossRef]

50. Parker, M.J.; Allen, M.A.; Ramsay, B.; Klem, M.T.; Young, M.; Douglas, T. Expanding the temperature range of biomimetic synthesis using a ferritin from the hyperthermophile pyrococcus furiosus. *Chem. Mat.* **2008**, *20*, 1541–1547. [CrossRef]

51. Lynch, I.; Dawson, K.A. Protein-nanoparticle interactions. *Nanotoday* **2008**, *3*, 40–47. [CrossRef]

52. Barui, A.K.; Oh, J.Y.; Jana, B.; Kim, C.; Ryu, J.-H. Cancer-Targeted Nanomedicine: Overcoming the Barrier of the Protein Corona. *Adv. Therap.* **2019**. [CrossRef]

53. Mosayebi, J.; Kiyasatfar, M.; Laurent, S. Synthesis, Functionalization, and Design of Magnetic Nanoparticles for Theranostic Applications. *Adv. Health Mater.* **2017**, *6*. [CrossRef] [PubMed]

54. Quanguo, H.; Lei, Z.; Wei, W.; Rong, H.; Jingke, H. Preparation and Magnetic comparison of Silane-Functionalized Magnetite Nanoparticles. *Sens. Mater.* **2010**, *22*, 285–295.

55. Mashhadizadeh, M.H.; Amoli-Diva, M. Drug-Carrying Amino Silane Coated Magnetic Nanoparticles as Potential Vehicles for Delivery of Antibiotics. *J. Nanomed. Nanotechnol.* **2012**, *3*, 1000139. [CrossRef]

56. Boyer, C.; Whittaker, M.R.; Bulmus, V.; Liu, J.; Davies, T.P. The design and utility of polymer-stabilized iron-oxide nanoparticles for nanomedicine applications. *NPG Asia Mater.* **2010**, *2*, 23–30. [CrossRef]

57. Sahoo, Y.; Pizem, H.; Fried, T.; Golodnitsky, D.; Burstein, E.; Sukenik, C.N.; Markovich, G. Alkyl Phosphonate/Phosphate Coating on Magnetite Nanoparticles: A Comparison with Fatty Acids. *Langmuir* **2001**, *17*, 7907–7911. [CrossRef]

58. Gupta, A.K.; Gupta, M. Synthesis and surface engineering of iron oxide nanoparticles for biomedical applications. *Biomaterials* **2005**, *26*, 3995–4021. [CrossRef]

59. Guardia, P.; Batlle-Brugal, B.; Roca, A.G.; Iglesias, O.; Morales, M.P.; Serna, C.J.; Labarta, A.; Batlle, X. Surfactant effects in monodisperse magnetite nanoparticles of controlled size. *J. Magn. Magn. Mater.* **2007**, *316*, e756. [CrossRef]

60. Frey, N.A.; Peng, S.; Cheng, K.; Sun, S. Magnetic nanoparticles: Synthesis, functionalization, and applications in bioimaging and magnetic storage. *Chem. Soc. Rev.* **2009**, *38*, 2532–2542. [CrossRef]

61. Fan, J.; Lu, J.; Xu, R.; Jiang, R.; Gao, Y. Use of water-dispersible Fe_2O_3 nanoparticles with narrow size distributions in isolating avidin. *J. Colloid Interface Sci.* **2003**, *266*, 215–218. [CrossRef]

62. Piñeiro-Redondo, Y.; Bañobre-López, M.; Pardiñas-Blanco, I.; Goya, G.; López-Quintela, M.A.; Rivas, J. The influence of colloidal parameters on the specific power absorption of PAA-coated magnetite nanoparticles. *Nanoscale Res. Lett.* **2011**, *6*, 383–389. [CrossRef] [PubMed]

63. Lu, X.; Niu, M.; Qiao, R.; Gao, M. Superdispersible PVP-Coated Fe_3O_4 Nanocrystals Prepared by a "One-Pot" Reaction. *J. Phys. Chem. B* **2008**, *112*, 14390–14394. [CrossRef] [PubMed]

64. Tombácz, E.; Farkas, K.; Földesi, I.; Szekeres, M.; Illés, E.; Tóth, I.Y.; Nesztor, D.; Szabó, T. Polyelectrolyte coating on superparamagnetic iron oxide nanoparticles as interface between magnetic core and biorelevant media. *Interface Focus* **2016**, *6*, 20160068. [CrossRef] [PubMed]

65. Yang, C.; Yan, H. A green and facile approach for synthesis of magnetite nanoparticles with tunable sizes and morphologies. *Mater. Lett.* **2012**, *73*, 129–132. [CrossRef]

66. Mornet, S.; Vasseur, S.; Grasset, F.; Duguet, E. Magnetic nanoparticle design for medical diagnosis and therapy. *J. Mat. Chem.* **2004**, *14*, 2161–2175. [CrossRef]

67. Gref, R.; Luck, M.; Quellec, P.; Marchand, M.; Dellacherie, E.; Harnisch, S.; Blunk, T.; Muller, R.H. 'Stealth' corona-core nanoparticles surface modified by polyethylene glycol (PEG): Influences of the corona (PEG chain length and surface density) and of the core composition on phagocytic uptake and plasma protein adsorption. *Colloids Surf. B* **2000**, *18*, 301–313. [CrossRef]

68. Rahman, M.; Laurent, S.; Tawil, N.; Yahia, L.H.; Mahmoudi, M. *Protein-NP Interactions, the Bio-Nano Interface*; Springer Series in Biophysics; Springer: Berlin/Heidelberg, Germany, 2013; Volume 15, pp. 21–44.

69. Pearson, R.M.; Juettner, V.V.; Hong, S. Biomolecular corona on nanoparticles: A survey of recent literature and its implications in targeted drug delivery. *Front. Chem.* **2014**, *2*, 108. [CrossRef]

70. You, J.O.; Almeda, D.; Ye, G.J.C.; Auguste, D.T. Bioresponsive matrices in drug delivery. *J. Biol. Eng.* **2010**, *4*, 1–15. [CrossRef]

71. Yadavalli, T.; Ramasamy, S.; Chandrasekaran, G.; Michael, I.; Therese, H.A.; Chennakesavulu, R. Dual responsive PNIPAM–chitosan targeted magnetic nanopolymers for targeted drug delivery. *J. Magn. Magn. Mater.* **2015**, *380*, 315–320. [CrossRef]

72. Dionigi, C.; Piñeiro, Y.; Riminucci, A.; Bañobre, M.; Rivas, J.; Dediu, V. Regulating the thermal response of PNIPAM hydrogels by controlling the adsorption of magnetite nanoparticles. *Appl. Phys. A Mater. Sci. Process* **2014**, *114*, 585–590. [CrossRef]

73. Digigow, R.G.; Dechéllez, J.F.; Dietsch, H.; Geissbühler, I.; Vanhecke, D.; Geers, C.; Hirt, A.M.; Rothen-Rutishauer, B. Preparation and characterization of functional silicahybrid magnetic nanoparticles. *J. Magn. Magn. Mater.* **2014**, *362*, 72–79. [CrossRef]

74. Vargas-Osorio, Z.; González-Gómez, M.A.; Piñeiro, Y.; Vázquez-Vázquez, C.; Rodríguez-Abreu, C.; López-Quintela, M.A.; Rivas, J. Novel synthetic routes of large-pore magnetic mesoporous nanocomposites (SBA-15/Fe3O4) as potential multifunctional theranostic nanodevices. *J. Mater. Chem. B* **2017**, *5*, 9395–9404. [CrossRef]

75. Ha, Y.; Ko, S.; Kim, I.; Huang, Y.; Mohanty, K.K.; Huh, C.; Maynard, J.A. Recent Advances Incorporating Superparamagnetic Nanoparticles into Immunoassays. *ACS Appl. Nano Mater.* **2018**, *1*, 512–521. [CrossRef]

76. Ito, A.; Hibino, E.; Shimizu, K.; Kobayashi, T.; Yamada, Y.; Hibi, H.; Ueda, M.; Honda, H.J. Magnetic force—Based mesenchymal stem cell expansion using antibody—Conjugated magnetoliposomes. *Biomed. Mater. Res. Part B* **2005**, *75B*, 320–327. [CrossRef]

77. Chao, C.; Jun, W.; Yong, Z.; Cong, L.; Lina, X.; Xin, Z.; Xiaolan, Y.; Ming, L.; Yang, B.; Tingyu, L.; et al. Improving Magnetofection of Magnetic Polyethylenimine Nanoparticles into MG-63 Osteoblasts using a Novel Uniform Magnetic Field. *Nanoscale Res. Lett.* **2019**, *14*, 90.

78. Chorny, M.; Fishbein, I.; Yellen, B.B.; Alferiev, I.S.; Bakay, M.; Ganta, S.; Adamo, R.; Amiji, M.; Friedman, G.; Levy, R.J. Targeting stents with local delivery of paclitaxel-loaded magnetic nanoparticles using uniform fields. *Proc. Natl. Acad. Sci. USA* **2010**, *107*, 8346–8351. [CrossRef]

79. Ryhänen, T.; Seppä, H.; Ilmoniemi, R.; Knuutila, J. SQUID magnetometers for low-frequency applications. *J. Low Temp. Phys.* **1989**, *76*, 287–386. [CrossRef]

80. Pankhurst, Q.; Hautot, D.; Khan, N.; Dobson, J. Increased Levels of Magnetic Iron Compounds in Alzheimer's Disease. *J. Alzheimer's Dis.* **2008**, *13*, 49–52. [CrossRef]

81. Tanaka, S.; Ota, H.; Kondo, Y.; Tamaki, Y.; Kobayashi, S.; Noguchi, S. Detection of magnetic nanoparticles in lymph nodes of rat by high Tc SQUID. *IEEE Trans. Appl. Supercond.* **2003**, *13*, 377–380. [CrossRef]

82. Adolphi, N.L.; Butler, K.S.; Lovato, D.M.; Tessier, T.E.; Trujillo, J.E.; Hathaway, H.J.; Fegan, D.L.; Monson, T.C.; Stevens, T.E.; Huber, D.L.; et al. Imaging of Her2-targeted magnetic nanoparticles for breast cancer detection: Comparison of SQUID-detected magnetic relaxometry and MRI. *Contrast Media Mol. Imaging* **2012**, *7*, 308–319. [CrossRef] [PubMed]

83. Bhuiya, A.K.; Asai, M.; Watanabe, H.; Hirata, T.; Higuchi, Y.; Yoshida, T.; Enpuku, K. Characterization of magnetic markers and sensors for liquid-phase immunoassays using Brownian relaxation. *IEEE Trans. Magn.* **2012**, *48*, 2838–2841. [CrossRef]

84. Cubells-Beltrán, M.D.; Reig, C.; Madrenas, J.; De Marcellis, A.; Santos, J.; Cardoso, S.; Freitas, P.P. Integration of GMR Sensors with Different Technologies. *Sensors* **2016**, *16*, 939. [CrossRef] [PubMed]

85. Osterfeld, S.J.; Yu, H.; Gaster, R.S.; Caramuta, S.; Xu, L.; Han, S.-J.; Hall, E.A.; Wilson, R.J.; Sun, S.; White, R.L.; et al. Multiplex protein assays based on real-time magnetic nanotag sensing. *Proc. Natl. Acad. Sci. USA* **2008**, *105*, 20637–20640. [CrossRef] [PubMed]

86. Chen, Y.T.; Kolhatkar, A.G.; Zenasni, O.; Xu, S.; Lee, T.R. Biosensing Using Magnetic Particle Detection Techniques. *Sensors* **2017**, *17*, 2300. [CrossRef] [PubMed]

87. Wang, W.; Wang, Y.; Tu, L.; Klein, T.; Feng, Y.; Wang, J.P. Surface Modification for Protein and DNA Immobilization onto GMR Biosensor. *IEEE Trans. Magn.* **2013**, *49*, 296–299. [CrossRef]

88. Lago-Cachón, D.; Rivas, M.; Martínez-García, J.C.; García, J.A. Cu impedance-based detection of superparamagnetic nanoparticles. *Nanotechnology* **2013**, *24*, 245501. [CrossRef]

89. Lago-Cachon, D.; Oliveira-Rodriguez, M.; Moyano, A.; Rivas, M.; Blanco-Lopez, M.C.; Martinez-Garcia, J.C.; Salvador, M.; Garcia, J.A. Scanning Magneto-Inductive Sensor for Quantitative Assay of Prostate-Specific Antigen. *IEEE Magn. Lett.* **2017**, *8*, 1–5. [CrossRef]

90. Moyano, A.; Salvador, M.; Martínez, J.C.; Rivas, M.; Blanco-López, M.C.; Gónzalez-Gómez, M.A.; Yáñez, S.; Piñeiro, Y.; Rivas, J. Carbon-coated superparamagnetic nanoflowers as labels in lateral flow imunoassays. In Proceedings of the 10th International Conference on Fine Particle Magnetism, Gijon, Spain, 27–30 May 2019; Book of Abstracts. p. 187.

91. Piñeiro-Redondo, Y.; Vargas-Osorio, Z.; Bañobre-López, M.; Kolen'ko, Y.V.; López-Quintela, M.A.; Rivas, J. Relevant Parameters for Magnetic Hyperthermia in Biological: Applications: Agglomeration, Concentration, and Viscosity. *IEEE Trans. Magn.* **2016**, *52*, 2300704(1-4).

92. Hergt, R.; Andrä, W. *Magnetism in Medicine: A Handbook*, 2nd ed.; Andrä, W., Nowak, H., Eds.; Chapter 4: Magnetic Hyperthermia and Thermoablation; Wiley-VCH: Berlin, Germany, 2007.

93. Minelli, C.; Lowe, S.B.; Stevens, M.S. Engineering Nanocomposite Materials for Cancer therapy. *Small* **2010**, *6*, 2336–2357. [CrossRef]

94. MagForce AG. Available online: https://www.magforce.com/en/home/our_therapy/ (accessed on 29 September 2019).

95. Dionigi, C.; Lungaro, L.; Goranov, V.; Riminucci, A.; Piñeiro-Redondo, Y.; Bañobre-López, M.; Rivas, J.; Dediu, V. Smart magnetic poly(N-isopropylacrylamide) to control the release of bio-active molecules. *J. Mater. Sci. Mater. Electron.* **2014**, *25*, 2365–2371. [CrossRef] [PubMed]

96. Santin, M.; Meikle, S.; Pineiro, Y.; Bañobre Lopez, M.; Rivas, J.; Santin, M. Mild hyperthermia nano-devices based on superparamagnetic nanoparticles conjugated with thermoresponsive poly(epsilon-lysine) dendrons tethered with carboxybetaine. *Acta Biomater.* **2016**, *40*, 235–242.

97. Chen, R.; Romero, G.; Christiansen, M.G.; Mohr, A.; Anikeeva, P. Wireless magnetothermal deep brain stimulation, Sciencexpress. *Science* **2015**, *347*, 1477–1480. [CrossRef]

98. Yue, K.; Guduru, R.; Hong, J.; Llang, P.; Nair, M.; Khizroev, S. Magneto-electric Nanoparticules for Non-Invasive Brain Stimulation. *PLoS ONE* **2012**, *7*, e44040. [CrossRef]

99. Carril, M.; Fernández, I.; Rodriguez, J.; García, I.; Peñadés, S. Gold-coated iron oxide glyconanoparticles for MRI, CT, and US multimodal imaging. *Part. Part. Syst. Charact.* **2014**, *31*, 81–87. [CrossRef]

100. Jang, J.-T.; Nah, H.; Lee, J.-H.; Moon, S.H.; Kim, M.G.; Cheon, J. Critical Enhancements of MRI Contrast and Hyperthermic Effects by Dopant-Controlled Magnetic Nanoparticles. *Angew. Chem.* **2009**, *121*, 1260–1264. [CrossRef]

101. Gupte, A.A.; Shrivastava, D.; Spaniol, M.A.; Abosch, A. MRI-related heating near deep brain stimulation electrodes: More data are needed. *Ster. Funct. Neurosurg.* **2011**, *89*, 131–140. [CrossRef] [PubMed]

102. Lee, N.; Choi, Y.; Lee, Y.; Park, M.; Moon, W.K.; Choi, S.H.; Hyeon, T.; Lee, J. Water-Dispersible Ferrimagnetic Iron Oxide Nanocubes with Extremely High r2 Relaxivity for Highly Sensitive in Vivo MRI of Tumors. *Nano Lett.* **2012**, *12*, 3127–3131. [CrossRef]

103. Zhao, Z.; Zhou, Z.; Bao, J.; Wang, Z.; Hu, J.; Chi, X.; Ni, K.; Wang, R.; Chen, X.; Chen, Z.; et al. Octapod iron oxide nanoparticles as high-performance T2 contrast agents for magnetic resonance imaging. *Nat. Commun.* **2013**, *4*, 2266. [CrossRef]

104. Wang, L.; Huang, J.; Chen, H.; Wu, H.; Xu, Y.; Li, Y.; Yi, H.; Wang, Y.A.; Yang, L.; Mao, H. Exerting Enhanced Permeability and Retention Effect Driven Delivery by Ultrafine Iron Oxide Nanoparticles with T1–T2 Switchable Magnetic Resonance Imaging Contrast. *ACS Nano* **2017**, *11*, 4582–4592. [CrossRef]

105. Adine, C.; Ng, K.K.; Rungarunlert, S.; Souza, G.R.; Ferreira, J.N. Engineering innervated secretory epithelial organoids by magnetic three-dimensional bioprinting for stimulating epithelial growth in salivary glands. *Biomater* **2018**, *180*, 52–66. [CrossRef] [PubMed]